



# IPN-ISD *Technology & Science* news

INTERPLANETARY NETWORK AND INFORMATION SYSTEMS DIRECTORATE

JET PROPULSION LABORATORY

September 2001 Issue 14

## In This Issue

**Charles  
Stelzried  
and  
Michael  
Klein**

*The name of the TMOD Technology and Science Program News has been changed to the IPN-ISD Technology and Science News. This is consistent with our recent JPL directorate name change from TMOD (Telecommunications and Mission Operations Directorate) to IPN-ISD (InterPlanetary Network and Information Systems Directorate). The following provides an overview of the articles. These are separated into three sections: Technology-Information Systems, Technology-Communications Systems, and Science.*

### Technology-Information Systems

Jefferey Srinivasan, et al., present an overview of reconfigurable processor technologies and a software reconfigurable network processor for space applications. The recon-

figurable processor performs all required receiver functions such as modulation, demodulation, error correction coding and decoding and will lead to an increase in the application of signal processing compared to traditional technologies. Missions considering the use of this technology include Space Technology 5 (ST-5) in 2003 and Mars Premier Orbiter in 2007.

A new computer algorithm for orbit trim maneuvers (OTMs) is described by Christopher Potts. These OTMs will be automated for future missions and will provide a robust and optimal solution without external ground user control. A prototype Automated Multiple Maneuver Optimization (AMMO) system has been developed which has demonstrated routine solutions while satisfying mission constraints. AMMO has been integrated with the navigation software approved for flight missions and has been satisfactorily tested with a preliminary Europa Orbiter trajectory. The planned transfer of AMMO into official navigation software and procedures is expected to reduce the future workforce for OTMs.

Jean Lorre and Eric DeJong are investigating a technique for tracking dynamic planetary and solar surface features. The history of these moving objects provides insight into the dynamics of their atmospheres. This may shed light on physical processes within the atmosphere. In certain cases, the spacecraft will transmit to Earth only the velocity vectors, providing a form of

## C O N T E N T S

Software Reconfigurable Processor Technologies	
The Key to Long-Life Infrastructure for Future Space Missions .....	3
Automated Multiple Maneuver Optimization (AMMO) .....	7
Solar Prominence Feature Tracking .....	12
Adaptive Optical Array Receiver	
Communicating through Atmospheric Turbulence .....	14
Bringing Data Back From Mars	
In Situ Communications Role — The Rover to Orbiter to Earth Link .....	21
Deep Space Station 13 Deep Space Network Research and Development, 34-m Beam Waveguide Antenna .....	28
Pre-College Student Contribution	
Cassini-Jupiter Microwave Observing Campaign (Cassini-JMOC) .....	35

data compression. Jean provides an autonomous means of modeling these giant loops.

### Technology-Communication Systems

Victor Vilmrotter and Meera Srinivasan describe improved ground-based reception of optical signals using a novel adaptive optical array receiver and optimum signal processing techniques. They propose collecting most of the signal energy while at the same time rejecting most of the interfering background collected by the receiver by means of a focal-plane detector array, operating jointly with a special purpose, real-time signal processing assembly. A hardware implementation is described and the performance of both an optimal array and a suboptimum array are evaluated. Results are described and the performance improvements reported. The simpler suboptimum detector array, with reduced complexity, performed nearly as well as the optimal array.

David Bell describes how an international fleet of spacecraft will explore Mars over the coming decade. This exploration is performed by orbiters, landers and rovers to conduct detailed in-situ investigations and the return of Martian samples to Earth for detailed laboratory evaluation. Deep space high-performance links from Mars orbiters, such as the MRO 2005 mission, will enable return of large science data sets. Proximity relay communications will piggyback these science orbiters to form a dedicated planetary relay satellite. Application of key IPN-ISD funded technologies such as ultra-low frequency, low-loss receivers and antennas

on the Mars surface-to-orbiter link will allow significant increases in data return while minimizing the user's energy-per-bit requirements.

Larry Teitelbaum describes the current Goldstone DSS 13, 34-m Beam Waveguide (BWG) antenna. Initiated as a project in 1987, this antenna was designed and constructed during 1988 and 1989. Seeing first light in 1990, DSS 13 was the first BWG antenna constructed in the DSN and has operated continuously for nearly a decade. Because the radio frequency beam is guided by microwave mirrors and reflectors from the Cassegrain focus to a focal point below the elevation axis, all sensitive electronics can be housed in an easily-accessed, non-tipping space protected from the weather. Since this instrumentation area is much larger than the cone of a typical Cassegrain antenna, additional equipment can be readily staged as well. Multiple research and development, microwave front-end systems at S, X, Ka and higher frequency bands are deployed and upgraded in this configuration with improved performance and lower-cost maintenance and operations.

### Science

The science article in this issue describes observations made by teenaged students of Jupiter's microwave radio emission during the Cassini Flyby of the giant planet earlier this year. Mike Klein and co-leaders led a team of scientists, educators and students in the ground-based measurements through the Goldstone-Apple Valley Radio Telescope (GAVRT) science-education partnership. The GAVRT observations revealed some unexpected changes in the intensity of Jupiter's radio emission. These will also provide useful data to validate the Cassini microwave receiver flight calibrations used for science observations when Cassini arrives at Saturn in 2004.



# Software Reconfigurable Processor Technologies

## The Key to Long-Life Infrastructure for Future Space Missions

### Abstract

We present an overview of long-life reconfigurable processor technologies and of a specific architecture for implementing a software-reconfigurable (software-defined) network processor for space applications. A prototype of the software-defined reconfigurable processor described here is currently operating in the laboratory at the Jet Propulsion Laboratory. The reconfigurable processor performs the functions of the physical layer (software radio), namely modulation, demodulation, pulse-shaping, error correction coding and decoding, as well as the data link layer, network layer, transport layer, and application layer science processing. The primary motivations behind the space-based, software-reconfigurable network processor are the following:

- To enable rapid-prototyping and rapid space-qualified implementations of communications, navigation, and science signal processing functions.
- To provide long-life communications infrastructure enabled by on-orbit processor reconfiguration.
- To provide greatly improved science instrumentation and processing capabilities through on-orbit, science-driven reconfiguration.

This work extends numerous advances in commercial industry as well as military software radio developments [1-5] to space-based radios and network processing. Such radios are software-defined while the implementation of the radio and other network functions are generally performed in combinations of the following software-defined processors: generic software processors, field

programmable gate arrays (FPGAs), digital signal processors, as well as traditional digital and mixed-signal applications specific integrated circuits and discrete analog-circuits. The development of such radios and the network processor presented here require defining the correct combination of the processing methods outlined above.

### Introduction

Many of the motivations for a space-based reconfigurable processor are similar to those driving reconfigurable processor efforts in private industry, in particular the cell-phone industry. Like cellular phones, space-based processors need long life, and during this lifetime, diverse applications arise. These potential applications cannot be anticipated at product/mission launch. Moreover, the value of adapting to these unpredictable needs is extremely high, driving the need for reconfigurability [1].

The reconfigurable processor architecture, a composite of the processors listed previously, is determined by making trades between complexity, cost, development time, mass and size, flexibility, power consumption, and reliability to achieve system requirements. Given the variety of processors available in the commercial sector and the varying development platforms, these trades are extraordinarily complex.

We present high-level design paradigms and a generic reconfigurable processor architecture for providing tremendous flexibility, which in this instance leads to long life, concurrent mission reconfigurability, and rapid prototyping of a wide variety of signal processing functions.

The high-level description of the functions of the space-based reconfigurable network

*Jeffrey  
Srinivasan,  
Allen  
Farrington,  
and  
Andrew Gray*

*Moreover,  
the value of  
adapting to these  
unpredictable  
needs is extremely  
high, driving the  
need for  
reconfigurability.*

processor is that it serves as communications infrastructure, science instrument and science data processor, and navigation infrastructure. Figure 1 is a conceptual illustration of these functions and how they are implemented. The network processor is represented in conventional network layers (layers 1-4, and 7 of the OSI network model).

Figure 2 illustrates a conceptual picture of the network layers implemented across a reconfigurable processor. This example assumes

a 1-million gate, Xilinx® field-programmable gate array and a 700-MHz Power PC processor. Note that the configuration of the software and hardware processors is defined by software control.

Figure 3 illustrates a new possible paradigm for communications, navigation, and science requirements developed by scientists and mission planners to be integrated into the network processor during an operational mission. Note that with reconfigurable pro-

Figure 1. Model of science, navigation, and communications processing

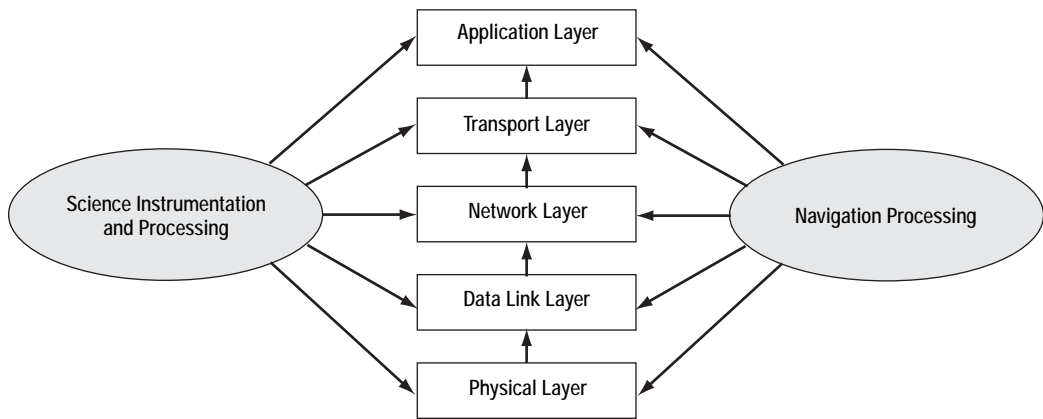
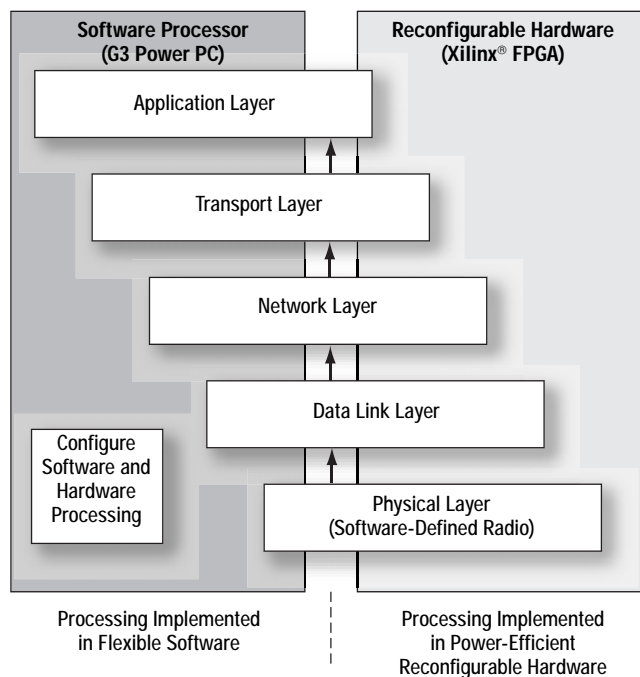
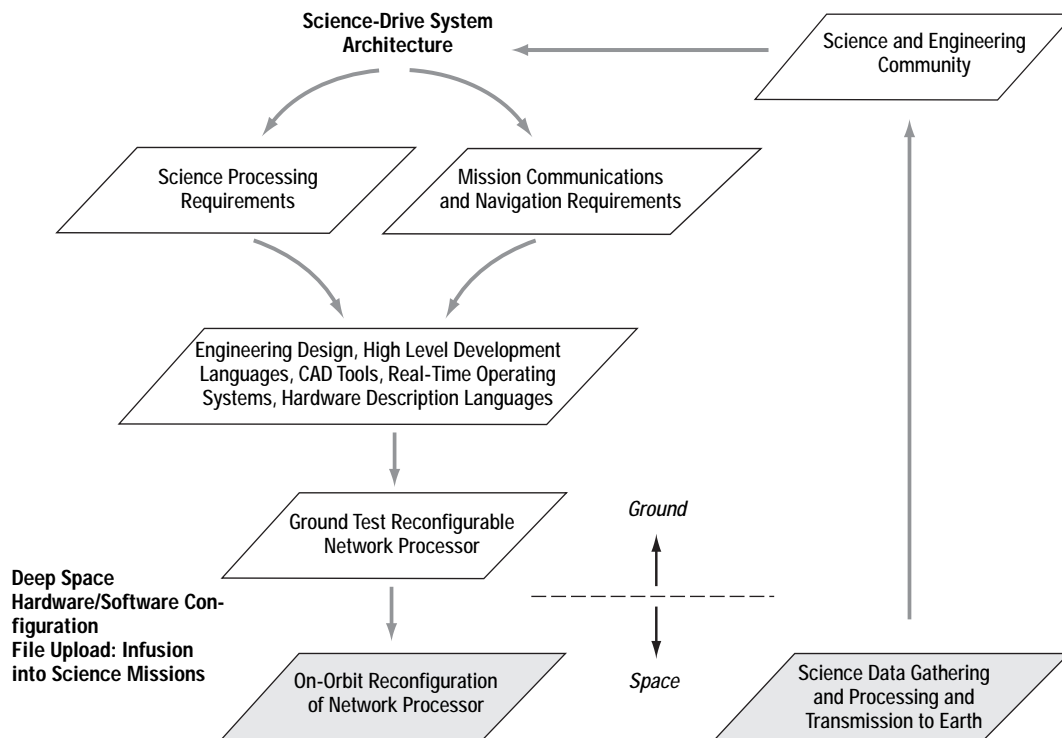


Figure 2. Network layers implemented in a reconfigurable processor





**Figure 3.**  
On-orbit  
reconfiguration  
of network  
processor

cessor technology, science processing may be modified by mission planners as a result of the science data acquired during a mission.

#### **Example: Physical Layer Software Radio**

The deep space communications channel has very unique problems compared to terrestrial communications. Primarily, the channel distances involved are often many orders of magnitude larger than those of terrestrial communications. This makes power-efficient transmission of information critical. Power efficiency may be increased through the use of error-control coding. Turbo-codes and low-density parity check codes currently offer performance approaching the Shannon limit on channel capacity [6]. The advantages these modern error-control codes exhibit over more conventional codes are well known and are on the order of many decibels in required transmit power savings. Unfortunately, the optimal decoders for many such codes are computationally intensive, making them prohibitively complicated to implement for high data rates. There is little doubt in the academic community that decoders for these

codes will be developed with significantly less complex implementations. In other words, although it would be a significant undertaking to implement a turbo decoder for data rates in excess of a few megabits per second in today's space-qualified processing technology, in a few years it is probable that simplified decoders will be developed to be readily implemented in this processing technology. Implementing such decoders in a processor years after launch is possible with the paradigm illustrated in Figure 3.

#### **Example: Navigation and Ranging**

The processor may be used to perform navigation functions. In some cases, the physical layer radio processing may need to be reconfigured to perform ranging. Using the paradigm of Figure 3, the modulation type processed by the physical layer and navigation algorithms processed by the application layer may be reconfigured from the ground.

#### **Example: Science Instrument Processing**

The argument for the need for on-orbit science processing enhancements is also

compelling. The science goals—and therefore the exact processing desired—may change after mission launch. An example of this was the desire to change the way occultation measurements were made in the CHAMP mission after launch. Mars Scout atmospheric occultation measurements may also reveal that changes should be made in the way these measurements are made.

The concept of the reconfigurable processor as a science-defined processor may be extended to include time-varying science processing. Due to the reconfigurable nature of the network processor it may fill the role of a large number of temporally-separated science instrument processors.

### Laboratory Prototype

A prototype of the reconfigurable processor illustrated in Figure 2 is currently operating in the laboratory. To date, the physical, data link, and transport layers have been implemented and demonstrated. The physical layer consists of a reconfigurable binary phase shift keying demodulator, the data link layer consists of an implementation of the majority of the Proximity-1 protocol draft recommendation by the Consultative Committee for Space Data Systems, and the transport layer consists of a commercial transport layer protocol. The processor has been demonstrated in a two-way communications link with data rates as high as 1 megabit per second per channel.

### Conclusion

We have provided a brief overview of software reconfigurable processor technologies and the paradigms used in development of the prototype software reconfigurable network processor operating in the laboratory at JPL. The authors believe reconfigurable processor technology leads directly to a tremendous increase in the diversity of applications of signal processing for science

benefits as compared to traditional processor technologies, and can provide long-life infrastructure support. Mission concurrent reconfiguration enables multi-mission support, reconfigurable communications and navigation infrastructure, and science instrumentation and processing improvements. Examples of missions considering to use the reconfigurable architecture of Figure 2 and variations developed at JPL include Space Technology 5 (ST-5) in '03, the Starlight instrument for Autonomous Formation Flyer in '06, and the Neige experiments on Mars Premier Orbiter in '07. The reconfigurable processor may also be appropriate for Mars Scout missions in '07 as well as future Mars Network payloads.

### References

- [1] N.J. Drew, M.M. Dillinger, "Evolution Toward Reconfigurable User Equipment," *IEEE Communications Magazine*, Volume: 39 Issue: 2, Feb. 2001
- [2] E. Buracchini, "The Software Radio Concept," *IEEE Communications Magazine*, Volume: 38 Issue: 9, Sept. 2000
- [3] W.H.W. Tuttlebee, "Software-defined Radio: Facets of a Developing Technology," *IEEE Personal Communications*, Volume: 6 Issue: 2, April 1999, Pages: 38-44
- [4] J. Mitola III, "Software Radio Architecture: A Mathematical Perspective," *IEEE Journal on Selected Areas in Communications*, Volume: 17 Issue: 4, April 1999 Pages: 514 -538
- [5] M.S. Cummings, S. Haruyama, "FPGA in the Software Radio," *IEEE Communications Magazine*, Volume: 37 Issue: 2, Feb. 1999 Pages: 108 -112
- [6] M. K. Simon, S. Hinedi, W. Lindsey, "Digital Communication Techniques," PTR Prentice Hall, Englewood Cliffs, New Jersey, 1995



# Automated Multiple Maneuver Optimization (AMMO)

## Introduction

Maneuver optimization was used extensively during tour operations for the Galileo prime mission about Jupiter. A new computer algorithm had been designed to assist in the process of designing orbit trim maneuvers (OTMs) such that the total spacecraft propulsive velocity change ( $\Delta V$ ) in the tour would be minimized while satisfying the mission constraints. Mathematical scale factors, or weights, were applied to the  $\Delta V$  components to obtain a nearly direct correlation between minimum  $\Delta V$  and minimum propellant consumption by the spacecraft. It was an exciting time to be involved with the maneuver optimization process and a rare opportunity to immediately apply the results of an optimization analysis to the actual spacecraft trajectory. Unfortunately, the optimization software involved a lot of initial setup, occasionally intense user interaction in the convergence process, cutting and pasting results between different programs, and in general a lot of trial and error.

Two main challenges exist to automate the maneuver optimization process for future missions. The first is to develop an algorithm for specific use in spacecraft operations that reliably converges on an optimal solution in the absence of any external user control. The second challenge is to incorporate the optimization algorithm into a complete automated system designed for robust spacecraft maneuver operations support over the entire mission.

Reliability and speed are critical characteristics of a maneuver and trajectory design system that will be exercised repeatedly during normal operations and with increased frequency as the spacecraft approaches critical mission events such as trajectory correction maneuvers (TCMs), gravity assist

flybys, orbit insertion burns, and encounter targeting. The system must also respond to unforeseen events like late orbit determination updates, spacecraft safe mode activities, and mission design changes. An additional bonus would be the ability to analyze case studies such as TCM Go/No-Go decisions or consider the cost to add an optional asteroid encounter to the interplanetary trajectory. Finally, the automated system should work nights, weekends, and holidays so that the analyst doesn't have to.

A prototype system has been developed to accommodate the repetitive nature of maneuver optimization in spacecraft flight operations. The Automated Multiple Maneuver Optimization (AMMO) system has been developed through the InterPlanetary Network and Information Systems Directorate (IPN-ISD) Technology Program in the Navigation and Radio Metrics work area. The prototype system has demonstrated the ability to routinely determine the optimal  $\Delta V$  requirements from updated orbit determination solutions while satisfying the mission specific constraints. The automated nature of the system reduces the design time requirements for commanded  $\Delta V$  by an order of magnitude. The demonstrated turnaround time is 15-30 minutes (depending on the complexity and duration of the trajectory), and subsequently the system is immediately ready to proceed with the next update. User interaction is not required, so the system is operational 24 hours a day/7 days a week for continuous maneuver design support.

## Optimization

The structure that defines the optimization problem and the linear optimization algorithm within AMMO was first used in operations during the Galileo mission [1-3].

**Christopher L. Potts**

*A prototype system has been developed to accommodate the repetitive nature of maneuver optimization in spacecraft flight operations.*

Determination of the optimal solution involves breaking the trajectory into discrete segments. A linear model of the segments is passed to the optimization algorithm along with a mathematical definition of the mission-imposed trajectory and maneuver constraints. The optimization algorithm performs a sequence of re-weighting iterations to determine the optimal solution to the linear model of the trajectory. The solution is applied to the original trajectory (which can be highly non-linear) and the process repeats until the numerically integrated trajectory segments produce a near-continuous trajectory. The trajectory segmenting and loop within a loop iterative approach has proven to be extremely flexible for a wide range of mission applications.

The AMMO algorithm provides the driver and controller of the optimization process to replace the interaction of an experienced user. When the solution to the linear approximation of the trajectory is applied to the original trajectory and numerically integrated, the discontinuities between trajectory segments can increase dramatically rather than decrease, as the linear solution would predict. Unfortunately, this is an all too common occurrence. The AMMO algorithm monitors this behavior and provides appropriate scaling of the linear solution to maintain the iterative path toward trajectory convergence. If necessary, the AMMO algorithm incrementally adjusts the bounds on the linear problem until it determines that the linear solution will improve the discontinuities in the original trajectory. AMMO has the capability to determine final trajectory convergence, and also identifies cases where the discontinuities can be reduced no further due to numerical precision limitations. The AMMO algorithm produces interactive feedback and control of the optimization process in a much more efficient and robust manner than even an experienced analyst can provide.

### **AMMO System**

After developing and improving a robust and automated optimization algorithm for use in spacecraft operations, the next step

was to integrate the capability with existing navigation software to demonstrate a prototype system for operations. The integrated system could then be applied and modified to accommodate an actual flight operations environment.

The AMMO system for operations is based upon the ability to start with a very good initial estimate of the optimal solution. Prior to flight operations, the mission design process defines the optimal reference trajectory. This nominal trajectory provides the initial estimates of the key control variables that define the reference mission. The task is to re-optimize the trajectory after incorporating new estimates of the initial spacecraft state and model variations. The spacecraft state and model updates result from the processing of navigation tracking data acquired in flight. With each optimization cycle, a new reference trajectory is created which provides initial control state estimates for use in the subsequent optimization. In this manner a good initial state estimate, which is generally critical for a reliable optimization solution, is routinely available during spacecraft operations.

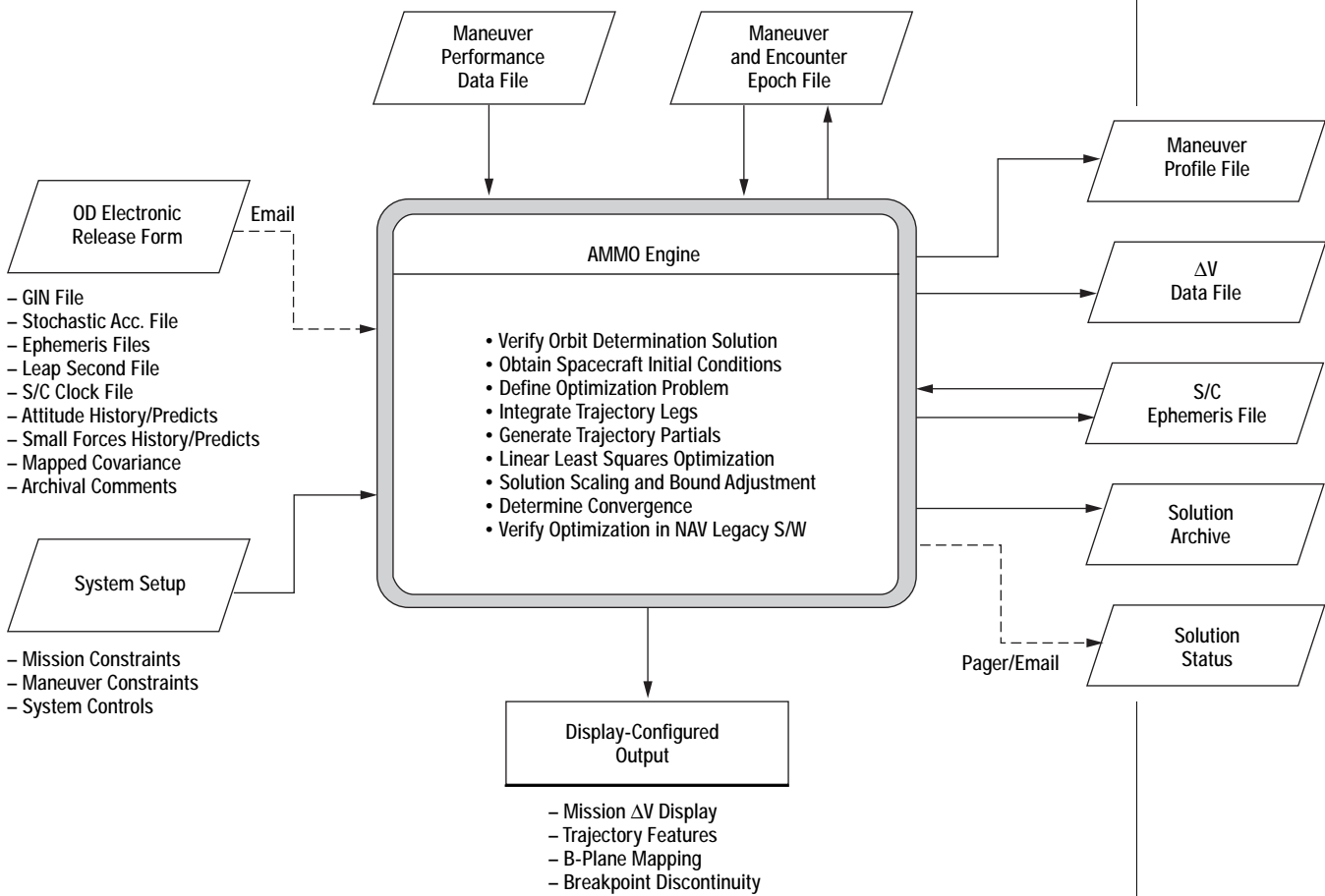
The focused nature of flight operations combined with a well-defined mission plan provide the framework to apply a software engine that will routinely determine the optimal  $\Delta V$  requirements from updated orbit determination solutions while satisfying the mission specific constraints. The software design accommodates mission inputs as opposed to individual maneuvers, and adjusts the optimization problem definition to fit the epoch of initial conditions as the mission progresses. Most of the model inputs to the software engine occur via standard file inputs. Hence, when a maneuver execution date changes, the date is manually changed in an existing maneuver epoch file and all subsequent AMMO solutions will utilize the new date. The AMMO engine constantly checks for notification of a new orbit determination (OD) solution. Currently, a new solution is delivered through a standard electronic form that includes all the navigation files that define the latest estimate of the spacecraft trajectory. The release form is sent

by email to the AMMO engine, which identifies the new delivery and immediately begins the re-optimization process.

The prototype AMMO software has been successfully integrated with the navigation software that has been approved for flight missions. While the optimization is occurring within the prototype software, the resulting targets are used as inputs to the navigation legacy software to verify the accuracy of the solution. The re-optimized trajectory results are usually available 15 minutes after the OD file is released. Numerous standard files are produced with each trajectory update. These include the maneuver profile file (commanded  $\Delta V$  for the next maneuver in the mission), a  $\Delta V$  data file of complementary information, and an updated

spacecraft ephemeris file spanning the end of the mission. An archive directory is created for each OD solution AMMO receives. If desired, a user can recreate and investigate any optimization result produced by AMMO. The AMMO system also creates status displays of the mission  $\Delta V$ , trajectory control events, a trajectory target plot, and graphical results to quickly observe the efficiency of the optimization process. Since the AMMO system is designed to operate continuously, the engine can send out a short email or alphanumeric page notification of the new  $\Delta v$  solution and the number of iterations required in the optimization process. Figure 1 shows a schematic of the AMMO system.

Figure 1.  
AMMO schematic



## Application

A preliminary Europa Orbiter trajectory provides the ultimate test to date for the AMMO optimization feedback and control algorithm. The highly non-linear trajectory includes approximately 60 trajectory correction maneuvers over a span of 4.5 years from launch to Europa orbit insertion. The dynamic trajectory contains 16 gravity assist flybys with altitudes as low as 100 km, two orbit insertion burns (Jupiter and Europa), two non-targeted flybys, and a highly-sensitive third body capture at Europa. Not surprisingly, applying the linear optimization algorithm to the entire trajectory proved to be numerically unstable. The AMMO algorithm is still able to control convergence in

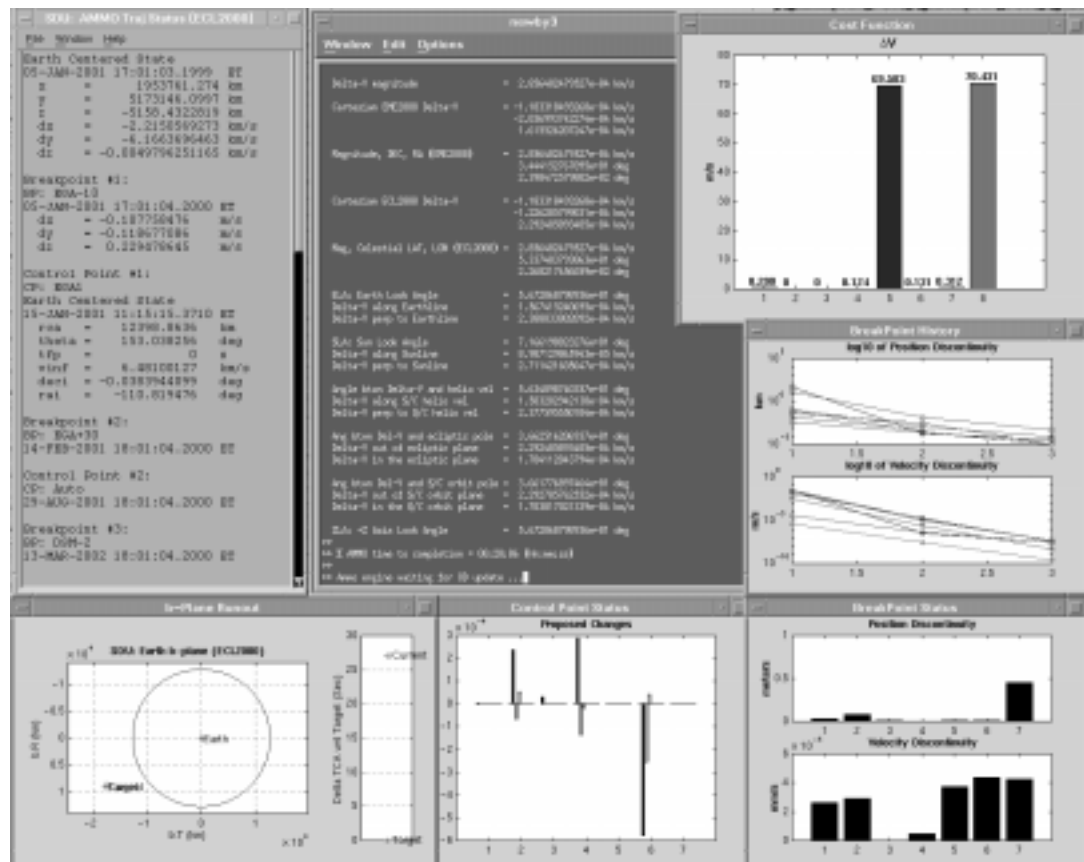
this extreme case. Even with the linear partials continually promoting a divergent solution, the feedback and control algorithm monitors and adjusts the linear bounds to achieve convergence.

From an optimization viewpoint, the Stardust mission trajectory is better behaved and a more stable problem. The AMMO algorithm monitors each iteration, but rarely needs to intervene by applying scale factors or adjusting bounds to the linear solution. The Stardust mission does provide an invaluable opportunity to test the entire AMMO system in a continuous spacecraft operations environment. For over a year now, the AMMO system has been supporting the Stardust mission. During this time, the AMMO system has received approximately 58 orbit determination solutions, and has generated a re-optimized Stardust trajectory usually within 15 minutes of the OD electronic delivery. The AMMO system has provided maneuver optimization support for the last three trajectory correction maneuvers

Figure 2.  
Dedicated AMMO terminal



Figure 3.  
AMMO display



(TCMs) including a rapid design schedule for the final Earth gravity-assist maneuver. The legacy navigation software generates the final TCM products based upon the AMMO optimization results. The TCM products receive a complete manual review before delivery, which is currently the most time-consuming aspect of the TCM design procedure. Figure 2 shows the X-terminal located in the Navigation Computing Facility devoted to AMMO for Stardust operations. Figure 3 shows the AMMO display results for a preliminary Stardust TCM design.

### Benefits

An automated ground system for maneuver design significantly reduces workforce requirements, saving time and money. The AMMO system has the potential to ultimately replace a maneuver analyst in the operational determination of trajectory correction maneuvers. The maneuver analyst can place more focus on the critical mission issues and less effort on the repetitive and time-consuming support task of re-optimization. In the current era of multi-mission support, additional efficiencies would result from using the same system for maneuver design across multiple projects. The AMMO capability can also be integrated as part of a complete automated navigation system, with future application toward an autonomous flight system [4].

The substantial time saving can also be transferred into mission performance improvements by utilizing shortened TCM design schedules. Later orbit determination tracking data cutoffs can be supported with subsequently-improved delivery accuracy for science benefit. For gravity-assist targeting, statistical  $\Delta V$  requirements are reduced as a result of improved delivery accuracy.

An automated system improves maneuver reliability and the efficiency of the design solution. The maneuver support level is elevated to 24 hours a day/7 days a week. Additionally, reference trajectory updates and the subsequent products become routinely available to support Deep Space Network predicts and sequence and science planning, for example.

### Summary / Future Plans

The prototype AMMO system has demonstrated the capability to routinely and automatically re-optimize the spacecraft trajectory in a flight operations environment. This capability has proven to be valuable during time-critical mission events and for extended maneuver analysis support with limited resources. Additionally, the control algorithm provides a systematic and relatively effective approach toward solving complex and numerically unstable trajectory optimization problems.

Future plans include a transition of the AMMO prototype capability into official navigation software and procedures. Currently, there is an ongoing effort to re-implement the legacy navigation software system with a modular design to promote future development efforts. Integration with this task will enable a more efficient AMMO implementation, and eliminate the dual modeling efforts that the prototype system requires to function with the current navigation software. In the meantime, maintenance of the prototype AMMO system improves operational efficiency, and eliminates the need for repetitive manual analysis.

### References

- [1] Byrnes, D. V. and Bright, L. E., "Design of High-Accuracy Multiple Flyby Trajectories Using Constrained Optimization," AAS Paper 95-307, AAS/AIAA Astrodynamics Specialist Conference, Halifax, Nova Scotia, Canada, 14-17 August 1995.
- [2] Lawson, C. L. and Hanson, R. J., "Solving Least Squares Problems," Classics Edition, Classics in Applied Mathematics 15, SIAM Books, (ISBN 0-89871-356-0), 1995.
- [3] Maize, E. H., "Linear Statistical Analysis of Maneuver Optimization Strategies," AAS Paper 87-486, AAS/AIAA Astrodynamics Specialist Conference, Kalispell, Montana, 10-13 August 1987.
- [4] Pollmeier, V. M., Burkhart, P. D., and Drain, T. R., "ARTSN: An Automated Real-Time Spacecraft Navigation System," Flight Mechanics/Estimation Theory Symposium, Goddard Space Flight Center, Greenbelt, Maryland, 1996.



# Solar Prominence Feature Tracking

*Jean J. Lorre  
and  
Eric DeJong*

## Introduction

Many images returned to Earth comprise objects with dynamic surfaces—Jupiter, Saturn, Venus, and the Sun, for example. Because these objects are constantly in motion, the history of where they move betrays the dynamics of the local atmosphere. From knowledge of atmospheric dynamics, we can reveal the physical processes at work within the atmosphere. In certain cases, it may be acceptable to permit spacecraft to track features and to return only the velocity vector-arrows that indicate the motion of an atmospheric feature over a period of time. This onboard type of logic has great potential in reducing the overall data transmission load to Earth. This algorithm takes feature tracking to a new level because it consists of a superposition of three-dimensional (3-d) hot loops—solar flare-types of features—upon a boiling background. There is benefit in characterizing solar activity because it directly affects communication on Earth. Great loops erupt from the Sun and eventually arrive here. We have found an autonomous means of modeling them.

## Modeling Prominences

One of the most interesting features we have been tracking has been solar hot loops seen in EUV (extended ultra violet) imagery. These features are more difficult to track than features lying on a surface because they appear different when viewed from various perspectives. Thus there is no way to predict feature locations in an image by just positioning the viewer or rotating the sphere. To obtain 3-d image structure, therefore, we must view the 3-d world via stereo image pairs.

With true (simultaneous) stereo pairs, and knowledge of where and when they were obtained, restriction of feature matching to those coordinates would produce physically

realistic solutions. Monocular views alone provide few constraints. In the process of matching features in stereo pairs in order to later track them, we compute the three-dimensional nature of these features, and can tell from their heights whether they are solar hot loops or surface structure. To illustrate, we determine the 3-d structure of hot loops and allude to possible data-compression benefits as follows.

First, solar coordinates, pointing coordinates, and camera parameters permit us to construct a “camera model.” A camera model is an algorithm that can convert a 3-d point in space into an image coordinate and, inversely, convert an image coordinate into a view ray from the camera into the 3-d space of the object. A view ray contains all those points in the 3-d object along your line of sight. Given a stereo pair with two camera models, we can construct an epipolar line. This is a line in both images formed by the plane containing both cameras and any 3-d point on or in the object being viewed. Epipolar lines are very useful because, given an image point in one camera, the only place the corresponding point can lie in the other camera is along the epipolar line defined by the first point. We will rely upon this formidable constraint to aid us in rejecting false matchings.

Then we process each image of the stereo pair independently. This involves locating points that are on the bright crest of hot loops, determining the direction of image texture, and then connecting the points together into strings representing individual loops.

We do not yet know the one-to-one (1:1) association between the strings sets in both images of this example. Therefore, to match the strings of points in both images, we compare each string in one image with the strings in the other image. For a point in one image we look for a string of points in the other image that cross the epipolar line. By comparing

*To obtain three-dimensional image structure, therefore, we must view the 3-d world via stereo image pairs.*

the view ray for the first point with the view ray for the epipolar crossing point in the other image, we extract the 3-d location of where these view rays cross. This will be a physical point in solar coordinates. If that point is on the solar surface, it belongs to a surface feature. If it lies within about 100,000 kilometers above the surface, it may be a point along a hot loop. If it is well above this or within the Sun, it is due to a mismatch between strings in both images and can be ignored. Many strings may cross the same epipolar line and result in nonphysical geometry. Eventually, after comparing all strings and tabulating all meaningful associations, matches are made based upon the number of good points in common between strings in both images. The result is a list of loops and their detailed 3-d profile in solar coordinates. This entire process is performed without human intervention.

It is not possible to test this process directly upon solar imagery because of the lack of simultaneous stereo pairs. Images taken close in time provide inadequate baselines and images taken far apart in time are unrelated. To test the software, we created synthetic hot loops using a magnetic solar model. Two such images are shown as Figures 1 and 2. The software locates all the shown hot loops and associates them correctly, producing 3-d values for each point that are close to the true synthetic ones. Only strings that are very close can be confused. We can, however, test the software that locates the strings of points. Figure 3 shows a trace image with strings superimposed, and in which many of the strongly linear features have been located.

We look forward to eventually tracking hot loops by locating features that look the same and propagate gradually with time.

### Data compression benefits

One potential benefit is in the area of data compression. If two satellites obtained stereo data then it would not be necessary to transmit the imagery to Earth. They could, on board the spacecraft, locate the strings of points lying along hot loops and downlink the strings. This would result in a data compression of about 1000 to 1 (1000:1).

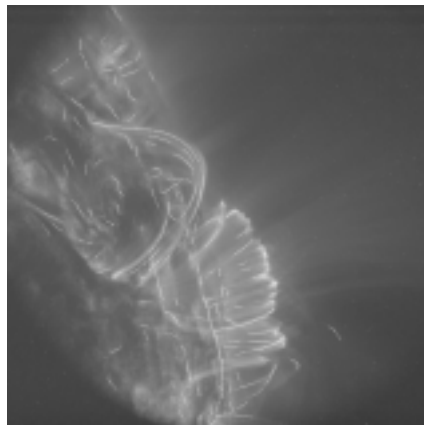
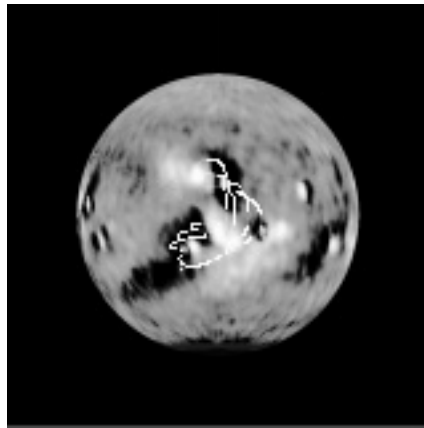
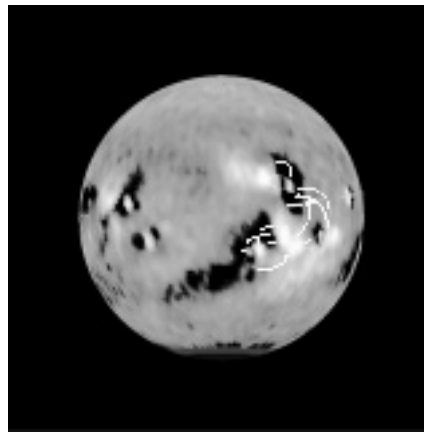


Figure 1.  
Synthetic hot loops  
using a magnetic solar  
model, Exhibit A

Figure 2.  
Synthetic hot loops  
using a magnetic solar  
model, Exhibit B

Figure 3.  
Trace image with  
strings superimposed

### Conclusion

There are many benefits to feature tracking in imagery of objects with gas atmospheres. These include autonomous feature recognition and modeling, and data compression based upon the specific topic of interest.



# Adaptive Optical Array Receiver

## Communicating through Atmospheric Turbulence

**Victor  
Vilrotter and  
Meera  
Srinivasan**

### Introduction

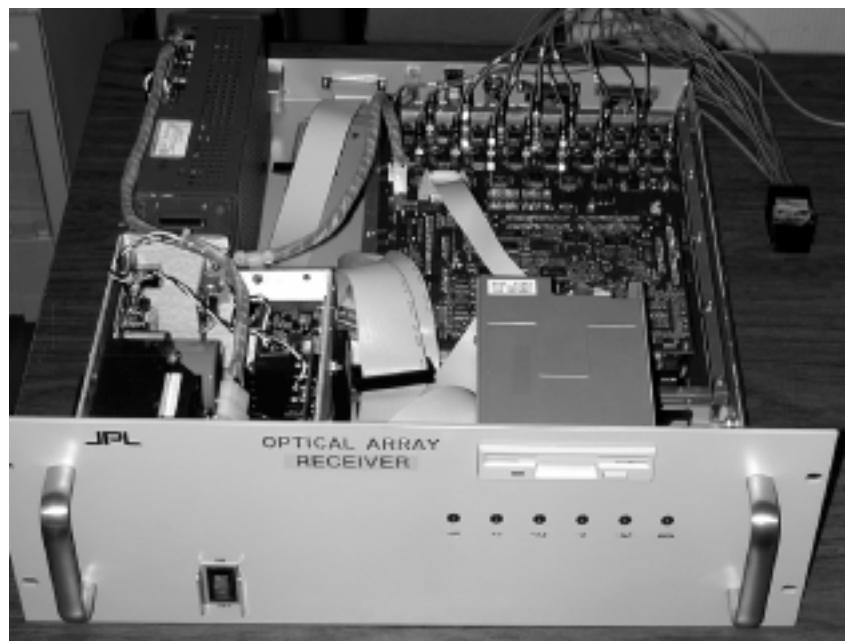
In this article, we describe a novel adaptive optical array receiver designed to improve ground-based reception of optical signals. The receiver is used to collect most of the incoming signal energy while at the same time rejecting most of the interfering background noise collected by the receiver. This requires a detector array placed in the focal-plane of the receiving telescope that operates jointly with a special-purpose signal processing assembly. The optimum processing method is to estimate the signal and background energies over each detector element in real-time, compute an optimum numerical multiplier called a “combining weight” to be applied to the output of each detector element, and sum the weighted outputs. However, for large arrays, these operations can become difficult to carry out at the required speeds; hence, a simpler, suboptimum “adaptive synthesized single detector” array receiver is also examined. A

breadboard implementation of this array receiver, employing a 16-element photomultiplier array and built by the Processor Systems Development Group (Section 335), is shown in Figure 1. With the performance of both the optimum and suboptimum array evaluated, the two receivers were shown to have comparable performance under operating conditions of interest. This article describes the atmospheric optical communications problem, an explanation of the algorithms needed to make these two adaptive receivers work properly, and a graphical description of their performance in terms of average probability of error.

### Atmospheric Effects

Ground-based reception of optical signals from space suffers from degradation of the optical signal field caused by atmospheric turbulence. This leads to a reduction in the

Figure 1.  
Breadboard Optical  
Array Receiver  
designed to  
demonstrate  
adaptive photon-  
counting array  
detection



effective diameter of the receiving telescope, and to random fluctuations of the receiver's point spread function (PSF) in the focal plane (the PSF describes how the signal energy is distributed in the focal-plane). Under ideal conditions, a tiny detector could be used to collect virtually all of the signal energy contained within the diffraction-limited PSF in the focal-plane, while at the same time spatially filtering out most of the background radiation. However, atmospheric conditions rarely permit diffraction-limited operation of large telescopes. Even under "good" night-time-seeing conditions, the phase of the received signal field tends to become uncorrelated over distances greater than 20 centimeters (cm), deteriorating to as little as 2–4 cm during the day [1]. Under these conditions, the dimensions of the PSF in the focal-plane tends to increase inversely with coherence length. This is as if the dimensions of a diffraction-limited telescope were correspondingly reduced. The telescope still collects all of the signal energy propagating through its physical aperture, but the signal energy is redistributed into a much larger spot in the focal-plane.

An example of the random redistribution of signal energy in the focal-plane due to turbulence is shown in Figure 2, superimposed on a  $16 \times 16$  array of detectors. By comparison, an ideally focussed spot would be mostly contained in a single-detector element.

#### *Optical Array Receiver Design*

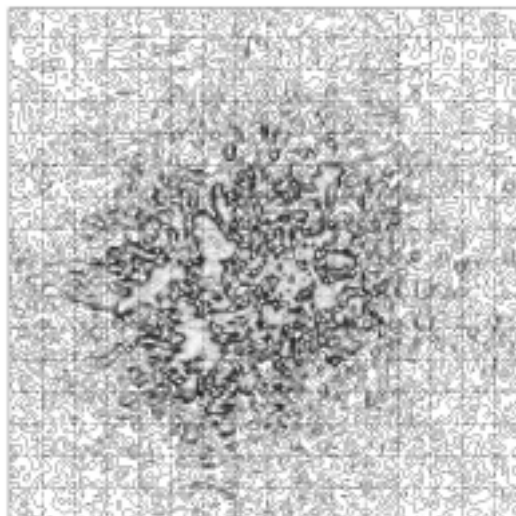
In order to collect most of the signal energy, the dimensions of a single optical detector must be made large enough to encompass the turbulence-degraded point-spread function as well as its random excursions in the focal-plane, which tend to change on time-scales of 10-100 milliseconds. However, a large detector implies a large receiver field-of-view. This in turn implies a corresponding increase in the amount of background radiation admitted into the receiver. That, in turn, degrades communications performance. These problems are effectively mitigated by the use of a

high-speed photon-counting detector array together with high-speed digital electronics capable of performing the signal-processing functions required for optimum or near-optimum receiver performance.

A conceptual block diagram of an optical photon-counting array receiver is shown in Figure 3. The receiver consists of a collecting aperture and optics to focus the collected fields onto the focal-plane, where a detector array counts individual photons generated by the impinging fields. The output voltages from every element of the array are converted to numbers, which are then processed by a high-speed, digital, signal-processing assembly that performs the required mathematical operations in order to optimize receiver performance.

#### **Optical Direct Detection with Focal-Plane Arrays**

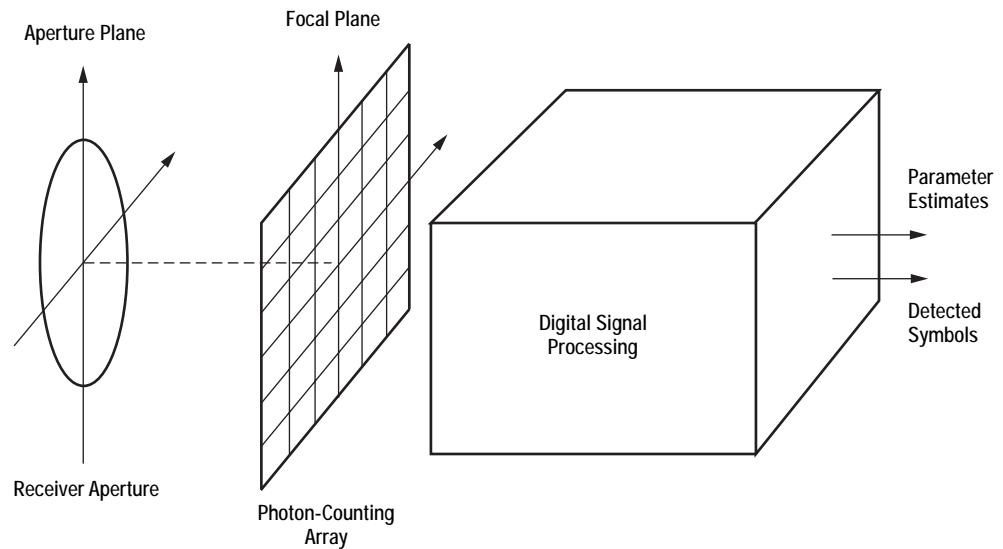
It has been shown in [2] that optical fields composed of a signal plus multimode background fields generate randomly-occurring pulses. These are approximately distributed, according to the Poisson probability density function, at the output of an ideal "photon-counting" detector. This model is reasonable for communications systems operating even at megabit-per-second rates. It also justifies the use of a relatively simple Poisson model, leading to mathematically tractable solutions. Using this model, two detector array receiver



*These problems are effectively mitigated by the use of a high-speed photon-counting detector array together with high-speed digital electronics capable of performing the signal-processing functions required for optimum or near-optimum receiver performance.*

**Figure 2.** Contour plot of instantaneous focal-plane signal distribution (covering  $16 \times 16$  array) due to atmospheric turbulence: 4-cm coherence length

**Figure 3.**  
Conceptual block  
diagram of optical  
“photon-counting  
array” receiver



algorithms have been investigated for use with a particular form of optical signaling considered for deep-space communications known as “pulse-position modulation” (PPM), namely, algorithms based upon an optimum detector array receiver and an “adaptively synthesized detector” subarray receiver.

#### *The Optimum Detector Array Receiver*

Pulse-position modulation (PPM) is an optical modulation format where a single optical pulse is placed into one of  $M$  consecutive time slots [4]. The received PPM symbol is decoded correctly if the value of the measurement corresponding to the signal-slot exceeds the measurement value from every other (non-signal) slot. The optimal photon-counting array observable consists of a numerically-weighted sum of all detector outputs, where the numerical weight for each detector element is a logarithmic function of the ratio of signal and background photon intensities. A single detector can be synthesized from the array by setting all of the weights equal to one. Limiting cases corresponding to receivers employing such a single photon-counting detector will also be considered for comparison.

#### *Adaptively Synthesized Detector Subarray Receiver*

In analyzing the optimal array, it was observed that detectors containing much more background energy than signal energy do not contribute significantly to the error probability, since the output of these “non-signal” detector elements are multiplied by weights that are very close to zero. This observation suggests the following suboptimum decoding algorithm which results in a greatly simplified receiver structure: list the detector elements starting with the one containing the most signal energy, followed by every other detector ordered according to signal energy. Compute the probability of error for the first detector element plus background, then form the sum of signal energies from the first two detector elements (plus background for two detector elements), and so on, until the minimum error probability is reached. Each of these sets of detectors may be considered to be a single detector, so that no weighting is applied to account for variations in the signal distribution over the detector elements included in a given set. The set of detector elements that achieves the minimum probability of error is the best “synthesized single detector” matched to the signal intensity distribution. In effect, the optimum logarithmic weights have been partitioned into two classes: “large” weights were assigned the

value one, while “small” weights were assigned the value zero. We will show that this simple partitioning achieves near-optimum performance in low-to-moderate background environments, but with greatly reduced decoder complexity. However, this straightforward process of performing the optimization by actually calculating the error probabilities for each partial sum of detectors is not practical. Some practical methods for approximating this procedure are described in greater detail in [5].

### Numerical Results

Both analytical calculations and computer simulations were performed to obtain PPM error probabilities for the optimally-weighted array and the adaptive synthesized detector subarray. In order to generate spatial distributions of the signal incident upon the detector plane, sample fields were generated using computer simulations as described in [6], resulting in a matrix of complex signal amplitudes. For the simulation, an atmospheric correlation length of  $r_0 = 4$  cm was assumed, which implies that the results should apply to any receiving aperture that is much greater than this correlation length [1]. The field intensity generated in the detector plane by the simulation was then integrated over the elements

of a  $16 \times 16$  detector array which encompassed the signal distribution in the detector plane. Constant average background energy was assumed over each detector element.

For a given sample function of the signal intensity distribution, the average signal energy over the  $16 \times 16 = 256$  detector elements was sorted in decreasing order, and M-ary PPM symbol error probabilities were calculated for increasing numbers of detectors, starting with the first detector. The lowest curve in Figure 4 shows the symbol error probability for binary PPM ( $M = 2$ ) as a function of the number of detector elements used, for the case  $K = 10$  and 0.1 (that is, total average signal photons absorbed by the entire array is 10, average number of background photons per detector element is 0.1). It can be seen that, for this case, the smallest error probability of 0.0049 is achieved by assigning unity weight to the first 15 detector elements containing the greatest signal intensities, and zero to all the rest. The other curves correspond to various “easily computable” functions that attempt to predict the best number of detector elements, as described in the Adaptively Synthesized Detector Subarray Receiver paragraph above, without actually having to compute error probabilities.

Symbol error probabilities for binary PPM ( $M=2$ ) are shown as a function of total aver-

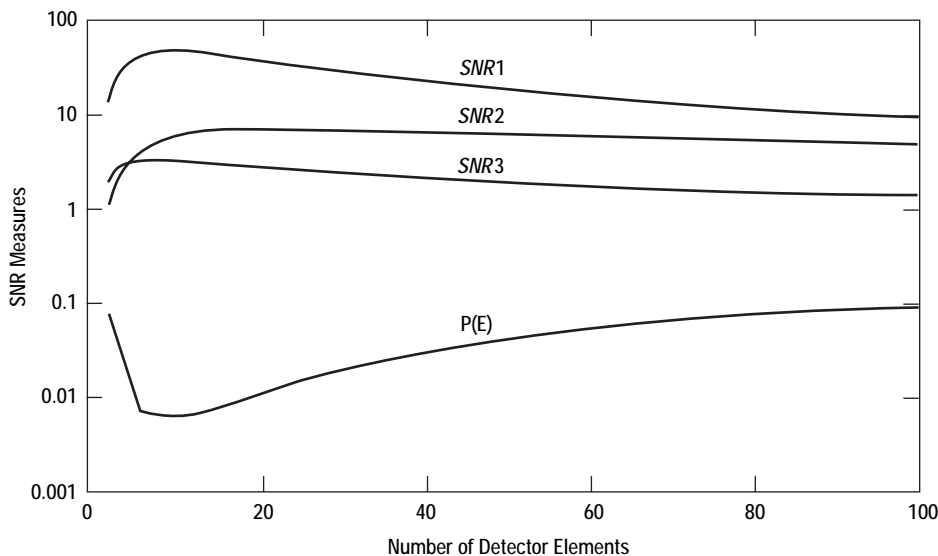


Figure 4. Comparison of the optimum number of detector elements and numbers predicted by the three SNR measures

age number of absorbed signal photons in Figures 5a and 5b, for the following cases:

- When the optimum number of “0-1” weighted detector elements are used
- Simulation of the optimally-weighted array
- When all 256 detector elements are given unity weight (synthesizing a large, nonadaptive single-detector element)
- When an ideal “adaptive optics” system succeeds in concentrating all of the available signal energy into a single-detector element, which then is the only detector element observed by the receiver.

The error probabilities computed in Figures 5a and 5b indicate performance gains by the adaptive synthesized detector subarray over a single, “large” non-adaptive detector of 2 and 2.8, respectively. This is at an error probability of 0.001, corresponding to 3 dB and 4.5 dB of performance improvement for average background photon counts of 0.1 and 1.0. When compared to the ideal “adaptive optics” receiver that concentrates all of the collected signal energy into a single element of the array, the gains are 3.8 and 8.2, corresponding to 5.9 dB and 9.1 dB of improvement. Note that the optimally-weighted array yields only about 0.3 dB improvement over the adaptive synthesized detector subarray at a symbol error probability of 0.001, even with very high background energy corresponding to  $K_b = 1$  background photon per detector element per slot.

Similar gains have been demonstrated for 16-dimensional ( $M = 16$ ) PPM, and documented in [5]. Results for higher dimensional PPM signaling including  $M = 2, 16$  and 256 are shown in Figure 6, plotted in terms of the receiver’s “photon efficiency” ( $\rho$ ), which is defined as the number of bits of information transferred by each photon on the average. Although 256 PPM is of great interest for possible use in future deep-space optical communications, the computation of exact error probabilities for this case were prohibitively complex; hence, only simulation results are shown for this case.

It can be seen that with background levels of 0.1 photons per slot, photon efficiencies of approximately half a bit per photon ( $\rho = 0.5$  bits/photon) can be achieved with 256 PPM signaling, at symbol error probabilities of 0.001–0.01. Additionally, coding can be applied to these PPM symbols to achieve even greater information efficiencies.

#### *Algorithmic Optimization of Number of Detector Elements*

One problem with the approach described above for determining the optimum number of detector elements is that computation of the error probability for each increasing subarray requires a great deal of time, particularly when large detector arrays are used, which may not be feasible in a real-time operational system. As an alternative, numerical measures that take into account the number of detectors and the total average signal and background energies were constructed to determine if simpler computations would suffice for determining the optimum number of detector elements in a real-time system. Three different measures were constructed and evaluated, each bearing some resemblance to a signal-to-noise ratio (SNR) although we emphasize that unlike for the case of additive Gaussian noise problems, in optical communications SNR is not necessarily a useful measure of performance. These three “easily computable” functions are defined in [5] and shown plotted in Figure 6 along with error probability. It can be seen that one of these functions, called  $SNR_1$ , yields performance comparable to that resulting from calculation of the exact error probability, but at a great savings in the required number of real-time computations.

#### *Estimation of Signal Intensities*

Finally, we note that the numerical results presented thus far were obtained under the assumption that the true values of the average signal and background photons absorbed by each detector element were known, and therefore the sorting of the detector elements was based upon the true signal energies. However, the signal energy distribution

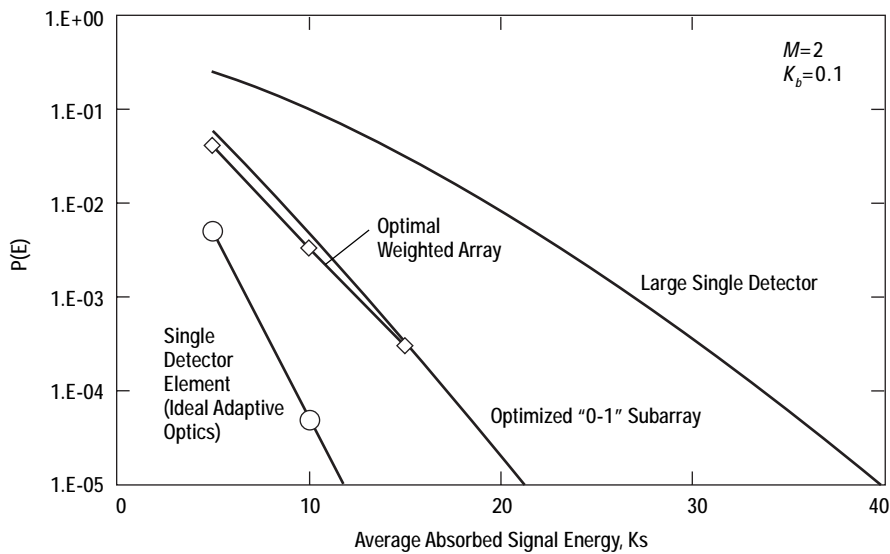


Figure 5a. Binary error probabilities for "large single detector," optimally-weighted array, adaptive synthesized detector subarray, and single detector element with ideal adaptive optics:  $K_b = 0.1$

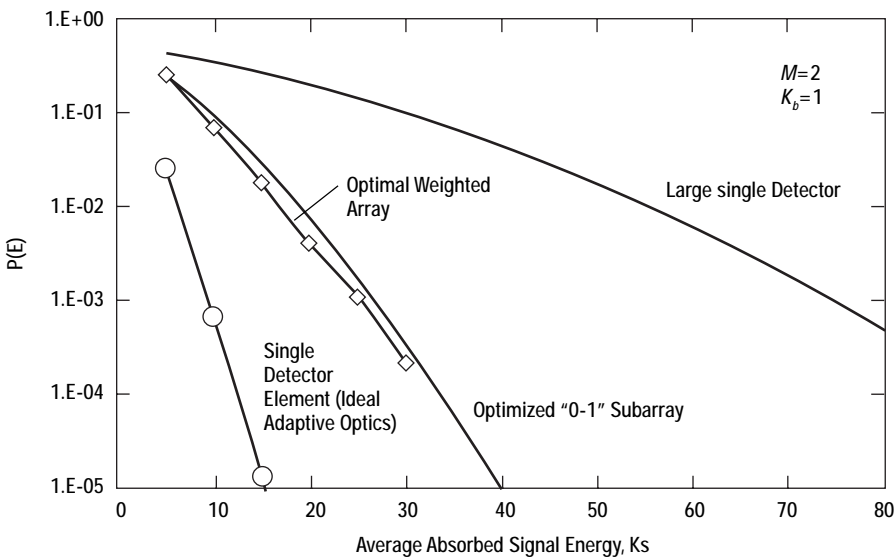
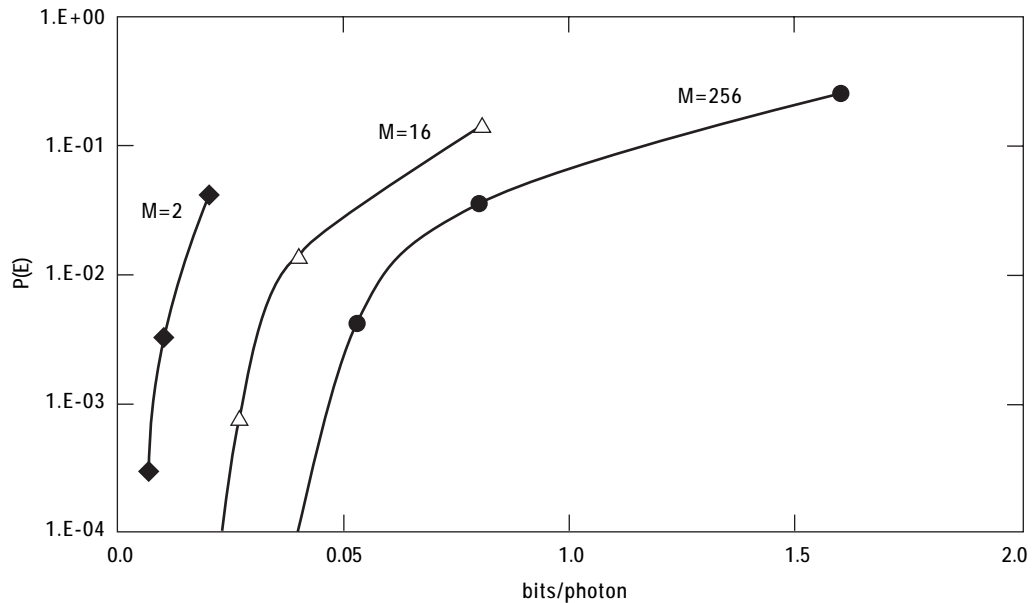


Figure 5b. Binary error probabilities for "large single detector," optimally-weighted array, adaptive synthesized detector subarray, and single detector element with ideal adaptive optics:  $K_b = 1$

changes with time due to turbulence, although the background intensity can be considered constant in most applications. Therefore, we also examined a case where the signal energies were not known a priori, but had to be estimated from the observed detector outputs. The results of simulations in which actual Poisson deviates were generated for each array element and the mean signal energies estimated from the observed outputs, are presented in [5].

For each detector array element, Poisson random variables were generated for the  $M$ -ary signal and background slots with average intensities obtained from computer simulations of the turbulent fields, plus a specified level of background light. These statistics were then sorted as before from largest to smallest. Both average number of signal and background photons were estimated from these statistics. We tacitly assumed that the actual background intensity

Figure 6. Simulated PPM bit error probability of optimum array receiver as a function of "photon efficiency"  $r$  (bits/photon),  $K_b = 0.1$



can be estimated accurately. This is because it is essentially, constant, in the detector plane and because typically there is significant "dead time" between PPM symbols to allow for transmitter laser recovery [4]. This can be used to estimate the background intensity directly since no signal photons whatsoever are present during these intervals.

Simulation results using these estimation algorithms demonstrate that that real-time estimation of signal energies over the array does not result in any appreciable performance degradation. It is also shown in [5] that subarray optimization based on the simple  $SNR_1$  algorithm mentioned above results in negligibly small losses but succeeds in greatly reducing the complexity of the estimator.

### Summary and Conclusions

A method of improving the performance of ground-based optical receivers in the presence of atmospheric turbulence through the use of photon-counting detector arrays and signal processing algorithms has been presented. Simulation results showed that use of an optimum array detection algorithm yields performance improvements of up to 5 dB relative to a single large detector designed to

collect most of the turbulent signal when operating in the presence of moderate to strong background radiation. It was also shown that in cases of interest, a simpler sub-optimum algorithm performed nearly as well as the optimum algorithm, with considerable savings in computational complexity.

### References

- [1] Andrews, L.C. and Phillips, R.L., "Laser Beam Propagation through Random Media," SPIE Optical Engineering Press, Bellingham, Washington, 1998.
- [2] Gagliardi, R.M. and Karp, S., Optical Communications, John Wiley & Sons, New York, 1976.
- [3] Snyder, D.L., Random Point Processes, John Wiley & Sons, New York, 1975.
- [4] Vilnrotter, V.A., Simon, M.K. and Yan, T.Y., "The Power Spectrum of Pulse-Position Modulation with Dead Time and Pulse Jitter," TMO Progress Report 42-133, Jet Propulsion Laboratory, May 15, 1998.
- [5] Vilnrotter, V.A. and Srinivasan, M., "Adaptive Detectors for Optical Communications Receivers," TMO Progress Report 42-141, May 15, 2000.
- [6] Negrete-Regagnon, P., "Practical Aspects of Image Recovery by Means of the Bispectrum," Journal of the Optical Society of America, Vol. 13, No. 7, July 1996.



# Bringing Data Back From Mars

## In Situ Communications Role — The Rover to Orbiter to Earth Link

### Introduction

Over the coming decade, an international fleet of spacecraft will carry out the most intensive exploration to date of another world in our solar system. A wide range of orbiters, landers and rovers will conduct detailed in situ investigations, culminating in an eventual return of Martian surface, subsurface, and atmospheric samples to Earth for detailed laboratory evaluation. Program success depends on the implementation of an orbital infrastructure to support the telecommunications and navigation needs of this mission set. (Definition of abbreviations and a glossary is provided at the end of the article.)

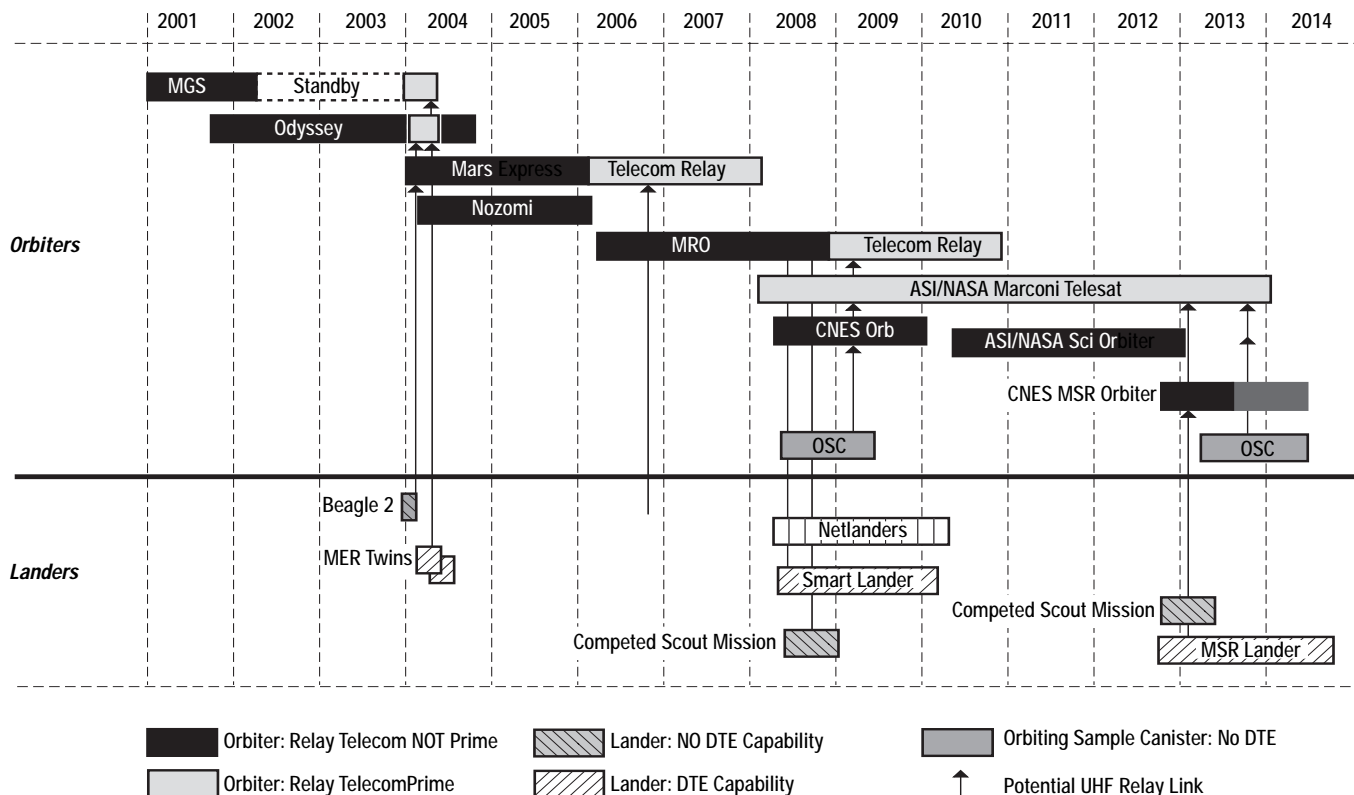
### Mars Program Overview

During 2000, a comprehensive replanning activity involving NASA and its international partners was carried out, establishing a new program of Mars exploration for the coming decade. The new plan incorporates program recommendations made after the loss of the Mars Climate Orbiter and Mars Polar Lander and integrates a systematic science strategy laid out by the Mars Exploration Payload Advisory Group.

A timeline of the planned mission set is illustrated in Figure 1.

*David Bell*

Figure 1.  
Mars exploration  
timeline



*For the smaller mission elements, Beagle 2 lander, Netlanders, Scouts and Orbiting Sample Canisters, the UHF relay telecom function is a mission enabler since they have no means to communicate directly to the Earth.*

Key elements of the program include:

- **Sample Return:** A driving element of the program is a planned Mars Sample Return (MSR) mission launched in the 2011 Mars launch opportunity. This mission would utilize a NASA lander to select, obtain and launch samples in an Orbiting Sample Canister (OSC). A CNES orbiter would retrieve the OSC and return it to Earth
- **Technology precursor missions:** Key MSR technologies include accurate pre-entry navigation, monitored entry/descent/landing (EDL), landing to an accuracy of 6 km or better, OSC orbit determination and rendezvous. The 2007 NASA "Smart Lander" and the 2007 CNES Orbiter missions will validate these and other key technologies prior to their use in the actual 2011 sample return.
- **Orbital reconnaissance:** To support site selection for sample return, in terms of both scientific and site safety considerations, the program includes a strong suite of remote sensing orbiters, including Mars Global Surveyor (MGS, NASA, '96), Mars Odyssey (NASA '01), Mars Express (ESA, '03), Nozomi (ISAS, '98), Mars Reconnaissance Orbiter (MRO, NASA '05), and CNES Orbiter ('07).
- **Competed scout-class missions:** In addition to the sample return mission and feed-forward technology precursor missions, the NASA program also incorporates competed scout-class missions, starting in the 2007 opportunity. These cost-capped, PI-managed missions are intended to broaden the science scope of the program and encourage innovative mission concepts that quickly respond to new scientific discoveries.
- **Telecommunication relay capabilities:** Recognizing the importance of telecommunications and radio-based navigation to the aggregate set of Mars missions, the program also provides proximity link relay telecommunications and navigation services based on an evolving orbital infrastructure. Near-term science orbiters such as Mars Global

Surveyor, Odyssey, Mars Reconnaissance Orbiter, and CNES' 07 will carry proximity link telecommunications payloads. In addition, the program includes the first dedicated Mars telecommunications spacecraft, the 2007 ASI/NASA Marconi telecommunications orbiter.

These UHF-equipped orbiter elements form the centerpiece of in situ telecom and navigation services for all other missions. The InterPlanetary Network and Information Systems Directorate in situ work area has focused on developing radio, antenna and coding technologies that will fly on orbiters and landed elements.

### Relay Orbiters Enhance Operations

For the smaller mission elements (Beagle 2 lander, Netlanders, scouts and OSCs) the UHF relay telecom function is a mission enabler since they have no means to communicate directly to Earth. For the larger landed elements, Mars Exploration Rover (MER), Smart Lander and MSR Lander/Rover, the UHF relay telecom can provide up to 10 times improvement in data return volume for the same (or less) expenditure of energy. For all of the missions, the orbiting infrastructure can provide navigation to assist in arrival and descent maneuvers as well as landed operations. Finally, the orbiting relays provide a link to the night side of Mars that is hidden from the Earth's view.

It is easy to see why a short-haul surface-to-orbiter relay link can outperform a direct to Earth link. Communication difficulty increases as range is squared. Mars-to-Earth range can reach a maximum of 2.7 astronomical units (AU) or 400-million km. Compare this to the in situ link ranges of 1000 to 6000 km. The power loss to Earth is over 100 dB greater than on the in situ link. This vast difference is difficult to make up even with the large Deep Space Network (DSN) antennas. Thus, the shorter haul surface-to-orbiter relay link can outperform a direct-to-Earth link by reducing energy

expanded, shortening pass times and dramatically increasing data rates and data volumes. Figure 2 below shows several examples.

The enhanced performance of the relay link requires that the relay spacecraft have sufficient data storage and Earth-link capacity so that it does not become a performance bottleneck. Figure 3 depicts a brief history of telecom performance from Mars and shows that there is significant performance headroom we can access with reasonable technology advancements. The X-band equipment currently proposed for the MRO mission provides a factor of 14 increase in data return relative to its precursor imaging mission MGS. Even with this dramatic improvement, both MRO and MGS are data-volume limited to imaging only 1% to 2% of the Martian surface at highest resolution. The MRO mission, at 30 cm per pixel resolution, generates 25 times more data than the 1.5 meters per pixel MGS camera when both spacecraft image the same surface area of the planet. Thus, from a science perspective, we are still quite data-rate-limited from Mars. The expectation is for future orbiters to continue to move to higher Earth-link

capacity via a combination of Ka-band, larger deployable antennas and higher traveling wavetube amplifier power. Onboard data storage capacity must also keep pace with the anticipated higher data volumes.

All of these advancements are beneficial to the evolution of relay telecom infrastructure. As Earth-link data rates increase, we have more room to improve the performance of the surface-to-orbit link without choking the Earth-link data pipe. Thus, the potential for high volume data return on a relay link increases, and the case for relay telecom, instead of direct-to-Earth data return, becomes stronger.

These data-rate calculations have been performed for maximum Mars-Earth range of 2.7 AU. As Mars-Earth range shortens to as little as 0.5 AU, the potential link capacity rises by a factor of 25x. For example, during the shorter-range portions of the MRO '05 mission, 1 AU or less, our potential long-haul Earth link rate exceeds 2 Mbps, and we move into an operating region where we are bandwidth- and equipment-limited rather than power-limited. A move to Ka-band will solve the bandwidth concerns, but

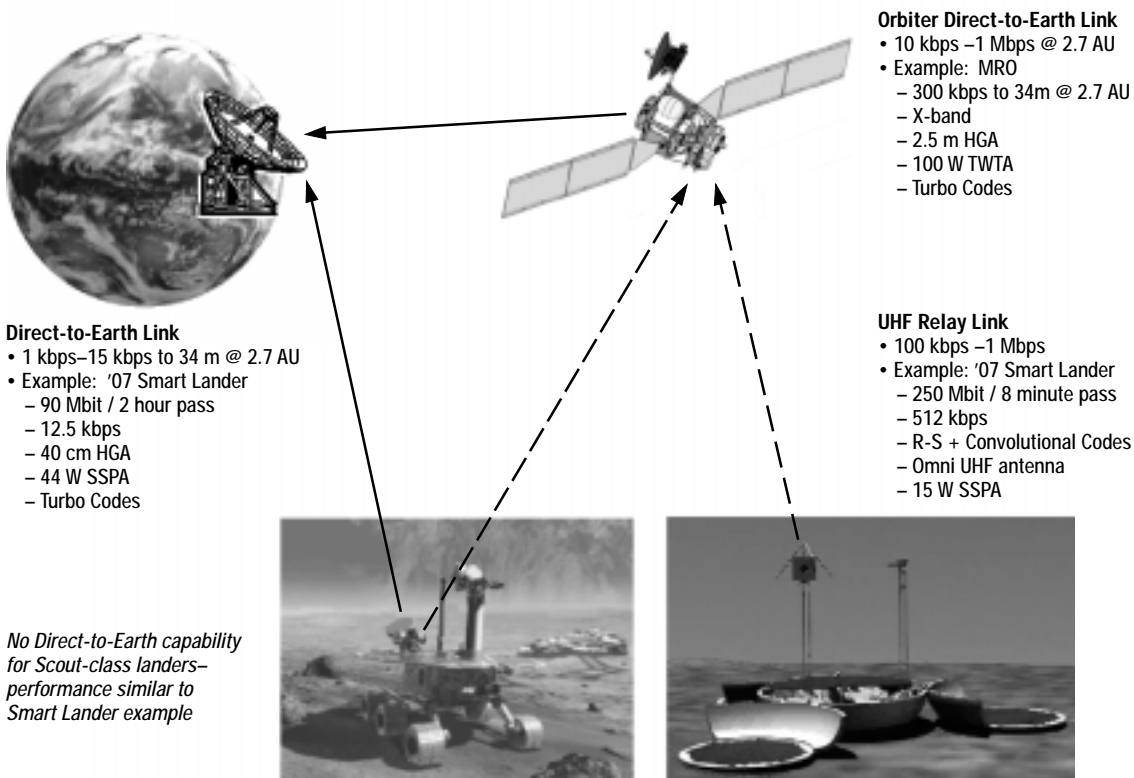
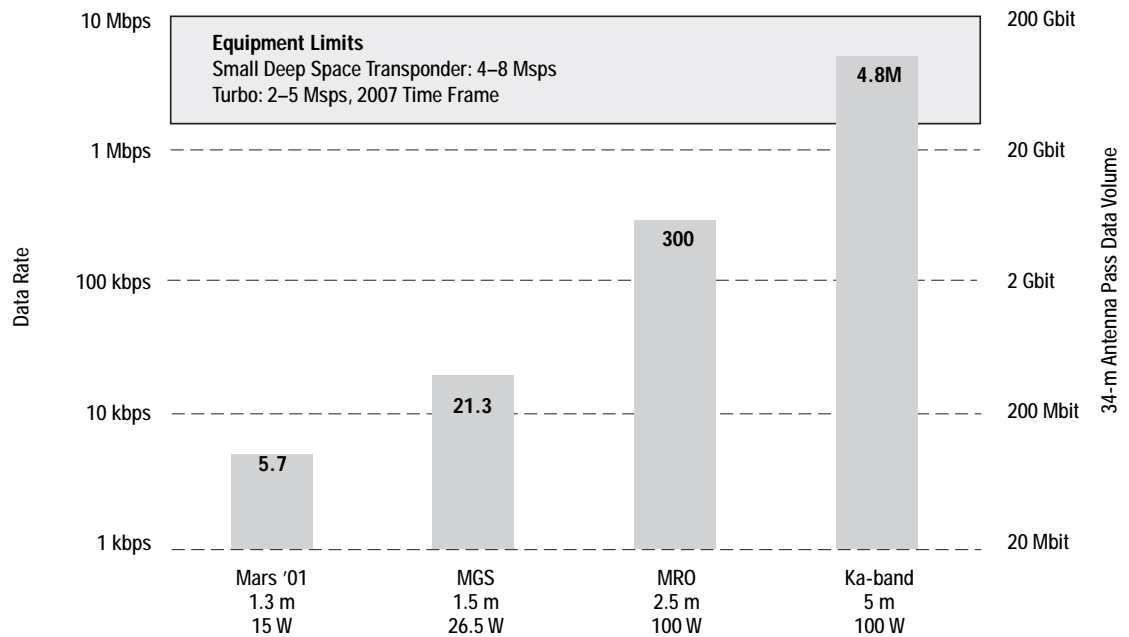


**Figure 2.**  
Relay links return more data than direct-to-Earth links

**Figure 3.**  
Past, present and  
future Mars Orbiter-  
to-Earth data  
capacities



Data volume assumes 40 minutes of occultation per 2-hour orbit. Yields 5.83 hours downlink time during a 10-hour DSN Pass.

pushes us further past the 2- to 8-megasymbols-per-second limits associated with the small deep-space transponder and near-term turbo decoders.

On the short-haul Mars surface-to-orbit link, it is again the orbiter equipment that can really pump up the performance. Figure 4 shows the expected evolution in surface-to-orbit link performance. The surface element performance is assumed to be constant at 15-Watts radio frequency (RF) and an omni-directional antenna. Increases in data throughput and data volume stem from the following design improvements.

*1) Lower loss receivers.*

Newer UHF Electra radio technology that will fly on the Mars Reconnaissance Orbiter, Mars '05, and later missions will operate with 2 dB lower filtering and radio losses compared to the older UHF relay radio design that is flying on Mars '01.

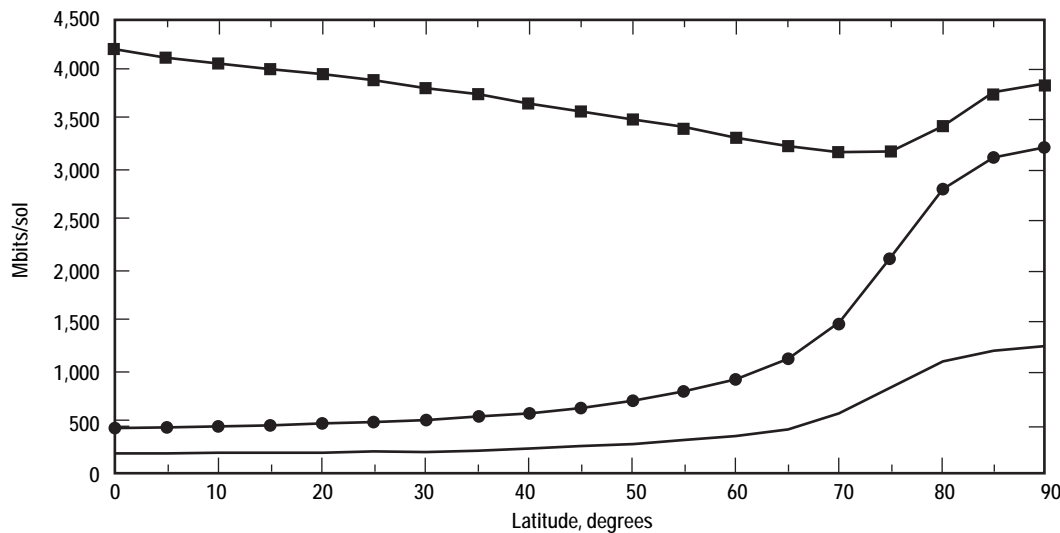
*2) Use of better channel codes on the relay link.*

Concatenating a (255,239) Reed-Solomon code to the standard rate 1/2 convolutional code improves the short-haul link performance by over 2 dB. IPN-

ISD technology development of onboard turbo decoders will add another 0.5 dB of performance improvement.

*3) Higher gain spacecraft antennas and longer pass times.*

The proposed joint Italian/NASA orbiter, Marconi, will be designed with relay telecom as the primary mission function. The 4450-km altitude, 130-degree inclination candidate orbit provides 3-5 passes per day to all Mars surface locations with an average per pass time of over 1 hour. This is a vast improvement compared to the low-altitude science orbiters that produce less than 3 passes per day with a typical duration of 7-8 minutes for surface sites below 45-degree latitude. Another advantage of the higher altitude non-polar orbit is that it provides coverage across 6-12 hours of Mars local "time zones." Thus, data can be returned at many different local times of day allowing for more operational flexibility. The lower altitude polar orbit used on science orbiters produce a narrow coverage swath that always views the same 2-hour local time zone.



**Relay Data Volume vs. Mars Surface Latitude**  
 — 15 Watt Xmit to Mar '01 400 km Orbiter, Conv Code Only, 0 dBi Receive Antenna  
 ● 15 Watt Xmit to Mar '05 400 km Orbiter, Conv + RS Codes, 2 dB better receiver, 0 dBi Antenna  
 ■ 15 Watt Xmit to ASI '07 4450 km Orbiter, Conv + RS Codes, 2 dB better receiver, 13 dBi Antenna

**Figure 4.**  
 Evolutionary improvements in surface-to-orbit UHF relay link capacity

A drawback of the higher altitude orbit is the longer slant range to users. This is compensated for in the design of the Marconi telecom orbiter by the inclusion of a medium gain, 13–15 dB power (relative to isotropic source), steered antenna. Several helix, yagi and array UHF medium-gain antennas are currently being studied under IPN-ISD funding. Compact storage, deployment and steering mechanisms are also part of these ongoing investigations in the IPN-ISD in situ telecom work area.

Again, the data volumes indicated above are potential numbers. If only the daytime passes are used, the data volumes are cut in half.

Are gigabits per sol from a single surface element required? Mission planners can certainly think up ways to use it. Initial planning on '07 Smart Lander and Sample Return missions include roving operations that will take one or more multi-spectral panoramic images every 100 meters along the traverse route. This corresponds to 1–2 images returned per sol. Even with moderate image compression, single images could exceed 1 gigabit (Gbit).

#### Electra Proximity Link Payload

For the past two years, IPN-ISD has funded the development of an in situ radio, the Micro Communications and Avionics System. MCAS has been selected as the core of JPL's next-generation proximity link payload, called Electra. Electra will provide telecommunications relay and in situ navigation services for future Mars missions. With a first flight on MRO, this payload could be flown on all subsequent Mars orbiters, provide de facto interoperability, and enable the gradual implementation of a Mars orbital communications/navigation infrastructure described earlier. Key high-level goals for Electra include:

- Flight reconfigurability to increase payload utility and accommodate new mission scenarios over long relay orbiter mission lifetimes
- Greater flexibility, including a wider range of supported data rates, swappable transmit/receive bands and simultaneous multi-channel operation
- Full compliance with Consultative Committee for Space Data Systems (CCSDS) Proximity-1 Link Protocol [CCSDS, 2000] and CCSDS File Delivery Protocol [CCSDS, 1999]

- Addition of X-band (8.4 GHz) receive capability, to support precision approach navigation, to support capture of EDL communications and to allow very high-rate reception of data from a lander equipped with a directional X-band DTE link
- Improved navigation/timing performance
- Improved communications link performance through addition of Reed-Solomon coding; low-loss, half-duplex operations mode; reduced receiver noise figure and increased power amplifier efficiency
- Modularity to allow scaling for low-mass lander/scout applications
- Portability to facilitate integration with a variety of orbiters and landed elements
- Self-contained relay functionality (including relay data management) for improved testability.

Current plans call for completion of an engineering model of Electra in early 2003.

### Summary

The coming decade of Mars exploration will demand improved telecommunications capabilities to meet the needs of a wide range of mission elements. Increased deep space link performance will enable return of large science data sets from high-resolution remote sensing orbiters such as the 2005 MRO mission. Proximity relay communications will piggyback on these science orbiters to form a heterogeneous constellation equipped with a standardized Electra communications/navigation payload, along with the first dedicated planetary relay satellite, the 2007 Marconi spacecraft. This orbital infrastructure must meet the diverse requirements of large, highly capable, second-generation landers/rovers as well as small, energy-constrained, scout-class missions. Application of key IPN-ISD funded technologies such as lower-loss receivers and increased gain UHF antennas on the orbiter and better channel coding on the surface-to-orbit link will allow significant increases in data return while minimizing the user's energy-per-bit requirements. The higher-altitude orbits being

considered for the Marconi spacecraft will increase temporal coverage for all Mars latitudes from minutes per day to hours per day, providing relay telecom users with much more operational flexibility and the potential of returning Gbits per day through the relay link.

### Abbreviations

The following abbreviations are used if not otherwise spelled out in this article.

<i>ASI</i>	Agencia Spaziale Italiana (Italian Space Agency)
<i>AU</i>	astronomical units
<i>CCSDS</i>	Consultative Committee for Space Data Systems
<i>CNES</i>	Centre National d'Études Spatiales
<i>dBi</i>	dB power relative to isotropic source
<i>DTE</i>	Direct to Earth
<i>EDL</i>	Entry, Descent, and Landing
<i>ESA</i>	European Space Agency
<i>Gbit</i>	gigabit
<i>HGA</i>	high-gain antenna
<i>IPN-ISD</i>	InterPlanetary Network and Information Systems Directorate
<i>ISAS</i>	Institute of Space and Astronautical Science
<i>kbps</i>	kilobits per second
<i>M/pixel</i>	meters per pixel
<i>Mbps</i>	megabits per second
<i>MCAS</i>	Micro-Communications and Avionics System
<i>MER</i>	Mars exploration rover
<i>MGS</i>	Mars Global Surveyor
<i>MRO</i>	Mars Reconnaissance Orbiter
<i>R-S</i>	Reed-Solomon
<i>SDST</i>	Small Deep Space Transponder
<i>SSPA</i>	solid-state power amplifier
<i>TWTA</i>	traveling wavetube amplifier
<i>UHF</i>	ultra high frequency
<i>yagi</i>	shortwave antenna

## Glossary

The following glossary may help understand terms used in this article.

### *Electra proximity link payload*

Electra is the name given to the next-generation UHF radio that will perform in situ communications between landers and orbiters. Just like science instruments, the Electra radio rides as a payload on a host spacecraft, lander or orbiter. Proximity link is a standard term used by the Consultative Committee for Space Data Systems, an international radio and communications standards group. There is actually a “CCSDS Proximity-1” protocol standard that will be implemented on the Electra radio.

### *In Situ communications*

Communications local to Mars. Mars landers and orbiters need to communicate with each other. The surface-to-orbiter link is used as the first hop-in relay communications to earth. A rover-to-lander link can be used. An orbiter-to-orbiter link might be used to collect radiometric information.

### *In Situ radio*

A radio designed specifically to operate with standards, frequencies and protocols specified for in situ communications.

### *In Situ telecom*

Same as In Situ communications above.

### *Orbiter relay link*

Meaning surface-to-orbiter relay link. It is a relay link because the orbiter serves as the relay point on the data pathway to Earth and the lander-to-orbiter portion is the first leg of the relay. We could also have a rover-to-lander relay link, the idea being that the lander acts as the relay point and the rover-to-lander link is the first leg of this relay link.

### *Pass time*

Interval of time that a landed element can see an orbiting spacecraft in the sky. During this time, the element can send data up to the orbiter and the event is called a “pass,” just like the DSN stations have 6–12 hour passes of objects they view in the sky. Pass times are usually referenced to some minimum elevation angle also; that is, the spacecraft must appear some minimum angle above the horizon before the pass starts, and the pass ends when the spacecraft falls below this minimum elevation angle as viewed by the surface elements.

### *Proximity link*

Another phrase for in situ link or in situ communications. A short-range communications or navigation radio link.

### *Proximity relay communications*

Same as described above, just different phrasing.

### *Relay link*

Same as described above, just different phrasing.

### *Relay telecom*

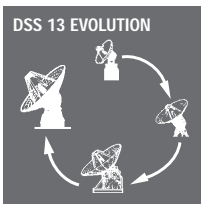
Same as described above, just different phrasing.

### *R-S + Convolutional codes*

To increase the performance of error correcting codes, they are often combined end-to-end. First, the data is Reed-Solomon (Irving S. Reed and Gustave Solomon) encoded, then it is convolutionally encoded. The short hand for such a concatenated coding scheme that involves Reed-Solomon and Convolutional codes is “R-S + Convolutional.”

### *Short haul surface to orbiter*

Short haul describes the “surface-to-orbiter relay link.” Short haul is in contrast to the long haul link to Earth—trucking terminology adopted by the communications community.



# Deep Space Station 13

## Deep Space Network Research and Development 34-m Beam Waveguide Antenna

*Lawrence  
Teitelbaum*

*The DSN has  
committed to the  
implementation  
of Ka-band, in  
support of the  
radio science  
objectives of the  
Cassini mission  
and future,  
high-rate  
telemetry.*

### Introduction

For many years, NASA's Deep Space Network (DSN) has relied on a research and development (R&D) antenna station for technology development, for demonstration and to prepare for the infusion of new capabilities into the operational DSN. Deep Space Station 13 (DSS 13) is both a logical concept and a physical realization appropriate to the needs of the DSN. The current manifestation of DSS 13 is a 34-m Beam Waveguide (BWG) antenna. Initiated as a project in 1987, DSS 13 was designed and constructed during 1988 and 1989, seeing first light in 1990. It was the first BWG antenna constructed in the DSN and has operated continuously for nearly a decade [Smith 1986, Britcliffe et al., 1991].

There were a number of motivations for upgrading DSS 13 from a 26-m Cassegrain telescope to a 34-m BWG antenna. The DSN required a stiffer antenna with a better surface to serve as a testbed for Ka-band. In addition, the DSN was interested in exploring the BWG concept both as an approach for the implementation of new apertures and as an option for retrofitting existing antennas to improve performance. Because the radio frequency (RF) beam is "guided" by microwave mirrors and reflectors, from the Cassegrain focus to a focal point below the elevation axis, all sensitive electronics can be housed in an easily accessed, non-tipping space protected from the weather. Since this instrumentation area is much larger than the cone of a typical Cassegrain antenna, additional equipment can be readily staged as well. This results in better performance at X- and Ka-bands and lower-cost maintenance and operations [Clauss and Smith, 1986].

DSS 13's initial role was to serve as a comprehensive testbed for all development

and implementation issues relevant to improving DSN capability by employing BWG technology and as the site for the push up in frequency to Ka-band. Its canonical role since has been:

- To provide a general test and demonstration environment for new microwave and system instrumentation concepts
- For automation and remote operations applicable to deep space communications
- To support scientific technology development and observation.

With the construction of the first of the operational BWG antennas—DSS 24, DSS 25 and DSS 26—the technology development emphasis shifted from the antenna itself to microwave instrumentation, performance improvement, and end-to-end ground system demonstration. The DSN has committed to the implementation of Ka-band in support of the radio science objectives of the Cassini mission and future high-rate telemetry. Optical communications has emerged as a potential, far future, even higher data-capacity telemetry channel. The station's current goal is to serve as the site for technology development leading to the future radio frequency DSN. DSS 13 is achieving this goal by:

- Operating as a frequency-agile instrument capable of world-class, ground-based radio astronomy, interferometry and radio science
- Implementing and refining a high frequency (> X-band [8 GHz]) observational capability, including gravity compensation for surface deformation
- Maintaining an ultra-low-noise capability, utilizing maser amplifier-based receivers

- Renewing its emphasis on automation, in particular, on increasingly autonomous ground station operations.

This vision has guided DSS 13 development and utilization for the last three years while, simultaneously, the station continues to play its canonical test and demonstration role.

### Capabilities

Similar to the operational BWGs, DSS 13 has a 34-m shaped-surface main reflector, with a center-fed beam waveguide. Its shaped-surface subreflector is supported by a tripod, which has been superseded by a more rigid, quadripod support on the operational antennas. Four intermediate mirrors reflect and focus the beam and deliver the RF signal to a large, subterranean, pedestal room located beneath the antenna mechanical structure. The pedestal room is stationary, unlike the main reflector, which must tip in elevation and rotate in azimuth to follow sources as they move across the sky.

As an R&D telescope, unlike the operational BWGs, DSS 13 has evolved from an open pedestal design, with a focal ring that now accommodates six, instrumented, feed-horn-and-receiver packages positioned on the pedestal floor. Sharing the same primary optics, RF energy can be directed at each of the feed positions in the focal ring by rotating a computer-controlled, ellipsoidal mirror. Final focus onto individual receivers is accomplished by flat mirrors, sometimes in conjunction with transmissive/reflective dichroic plates for simultaneous, dual-frequency operation. The DSS 13 antenna structure and complete optical path are illustrated in Figure 1.

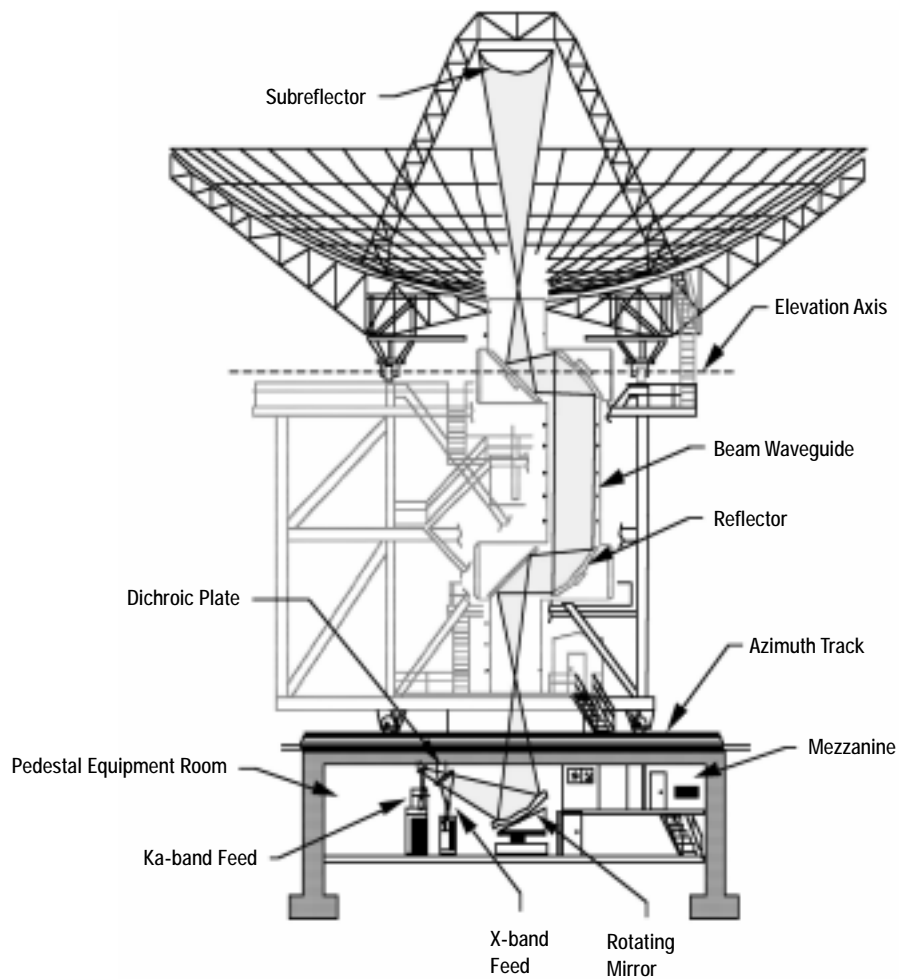
DSS 13's servo, encoder and antenna control subsystems were upgraded in 1998 to the emerging DSN standard antenna-pointing controller, the APC. The APC has been implemented on the operational BWGs and will be delivered on the high efficiency (HEF) and 70-m antennas by 2003. One of the challenges facing DSS 13 is maintaining sufficient compatibility with the rest of the DSN so that new DSN systems can be readily

staged at the facility for subsystem, integration and end-to-end testing. Embracing new technology in fundamental systems that is subsequently not adopted by the DSN can also leave DSS 13 out of step with the operational network, impairing the station's ability to play its test and integration role.

DSS 13's richest asset—and what distinguishes it most from its operational counterparts—is its extensive set of front-end feed horns and receivers. Presently, there are ten operable receivers in residence at the station:

- 1) *S-/X-band (2/8 GHz) dual-frequency Very Long Baseline Interferometry (VLBI) receiver*: Standard DSN VLBI dual-frequency package in a single refrigerator. Selectable right- or left-circular polarization (RCP or LCP)
- 2) *DSN X-band (8 GHz) receiver*: Standard DSN single polarization (RCP)
- 3) *X-band (8 GHz) ULNA radar receiver*: Liquid helium-cooled maser, simultaneous dual polarization (RCP/LCP)
- 4) *Ku-band (13.8 GHz) Cassini-JMOC receiver*: Developed in collaboration with the Goldstone-Apple Valley Radio Telescope project (GAVRT), a science education outreach activity, for the Cassini-Jupiter Microwave Observing Campaign (JMOC). Matched in frequency to the Cassini radar instrument
- 5) *K-band (22 GHz) Dicke beam-switch receiver*: Dual horn, three channel package, operable either in simultaneous dual polarization (RCP/LCP) mode or in single polarization, beam-switch mode
- 6) *Ka-band (32 GHz) monopulse receiver*: Single polarization (RCP) with integrated monopulse tracking coupler for closed-loop, precision spacecraft pointing
- 7) *Ka-band (32 GHz) broadband low-noise receiver*: R&D modification of the DSN's first Ka-band receiver
- 8) *Ka-band (34 GHz) Zeeman maser receiver*: Liquid helium-cooled maser, simultaneous dual polarization (RCP/LCP) [Levin and Hofhine 2000, Levin et al., 2001]

Figure 1.  
DSS 13 antenna  
structure



9) *Q-band (43 GHz) R&D receiver:* Cryogenically cooled high-electron-mobility (field-effect) transistor (HEMT), simultaneous dual polarization (RCP/LCP).

10) *W-band (90 GHz) R&D receiver:* Currently under development as a collaboration between InterPlanetary Network and Information Systems Directorate (IPN-ISD) Technology program and DSN radio astronomy.

Detailed front-end specifications for all the receivers resident at DSS 13 can be found on the station's web page at <http://Ntserve.gdsc.nasa.gov/13site.html>

DSS 13 maintains a modest transmit capability for uplink, a 20 kilowatt (kW) trans-

mitter at X-band and an 80 watt (W) transmitter at Ka-band (34 GHz). Although limited in power, until quite recently DSS 13 possessed the only Ka-band uplink available in the DSN.

Intermediate frequency (IF) signals are routed from the pedestal via a  $16 \times 4$  channel IF matrix switch. The selected IF channels are transmitted over optical fibers to the control room where they can be distributed to a number of back-end processors:

- Precision, two-channel radiometer
- Full-spectrum recorder (FSR)
- Radar downconverter
- Wide-Band Spectrum Analyzer (WBSA)

- VLBI MkIV Data Acquisition Terminal (MkIV DAT). The station's VLBI capability is complemented by the Real-Time Block II correlator (RTB2), a device that can take formatted data streams from two MkIV DATs and extract interferometric fringes in real time, thus constituting a connected-element interferometer (CEI).

Six optical fibers connect DSS 13 to Goldstone's main signal-processing center (SPC 10):

- Two fibers carry precision frequency and time information to DSS 13 from SPC 10
- Two normally deliver radar data from the DSS 13 radar downconverter to SPC 10 radar processors
- One delivers IF data from DSS 14, the 70-m antenna, to DSS 13's microwave spectrometers
- One is dedicated to bringing formatted VLBI data from SPC 10 to the RTB2.

Note that there is no reference to a telemetry capability. DSS 13's telemetry capability has not been upgraded since the prototypes of the Block V Receiver (BVR) were tested at the station. Because of the initial hardware cost hurdles, renewal of DSS 13's downlink telemetry capability has not been accomplished.

The monitor and control environment (M&C) at DSS 13 has been transformed over the past two years to support the transition to the APC, to provide a foundation for automation and remote observing, and to bring the station into conformity with the Research & Development Control System (RDC). The RDC is an R&D community-uniform architecture for data acquisition, antenna command and control, and automation used by DSN Science, VLBI and R&D elements of the DSN at all three operational complexes. The RDC is comprised of the Equipment Activity Controller (EAC), the Radio Astronomy Controller (RAC), the PC Field System (PCFS), and interfaces for M&C and messaging. The EAC serves as the station master controller, as a gateway to

DSN-standard subsystem controllers, and as an automation engine. The RAC controls instruments such as ambient loads, noise diodes, power meters and synthesizers. The PCFS is the MkIV DAT and VLBI execution controller. A challenge facing the M&C at DSS 13 is that the station depends on the RDC for its automation effort and for science observing while simultaneously striving for compatibility with the future M&C environment currently planned for the DSN, the Network Monitor & Control (NMC).

### Recent Accomplishments

DSS 13 has been instrumental in the development of nearly all the ground station technologies required by the radio science experiments to be conducted by the Cassini mission, as well as validating the performance of the onboard instrumentation dedicated to radio science:

- The monopulse tracking coupler, a closed loop, feedback-driven system for precise antenna pointing, was demonstrated at DSS 13. It has since been transferred to operations as an embedded element of the monolithic X/X/Ka receiver
- The beam aberration and point-ahead system was required to offset the transmit and receive beams. This was to compensate for tangential spacecraft motion during the long, round-trip light times to Cassini. The system was first demonstrated at DSS 13 and has been transferred to operations
- The Cassini media calibration system, in particular, the Advanced Water Vapor Radiometer (AWVR) which is critical to the Gravity Wave Experiment, was validated by the CEI-AWVR comparison experiment carried out with simultaneous observations from DSS 13 and DSS 15. The exceptionally radiometrically-stable receiver from the AWVR was used to explore the BWG-embedded AWVR concept. This activity pioneered the use of a potential seventh "suspended" feed position by hanging the receiver from the pedestal room ceiling and looking directly at the ellipsoid

- A critical, in-orbit instrument checkout that used DSS 13's Ka-band uplink:
  - confirmed the functionality of the Cassini Ka-band translator
  - demonstrated the first Ka-band downlink coherent with a Ka-band uplink
  - demonstrated the first, three-link configuration (simultaneous X-band/Ka-band downlink coherent with X-band uplink).

The prime observing phase of Cassini-JMOC recently concluded. Using a receiver developed specifically for this work and matched in frequency to the 13.8-GHz Cassini Radar instrument, JMOC measured Jupiter's microwave emission from the ground while similar measurements were made from the spacecraft. The observations were conducted remotely by students throughout the nation under the auspices of the Goldstone-Apple Valley Radio Telescope (GAVRT) project. The GAVRT project is a science outreach collaboration between JPL and the Lewis Center for Educational Research. The strong synergy between GAVRT's remote operation model and DSS 13's automation objectives significantly accelerated the station's transition to the remote, unattended observing mode. JMOC's need for a precise, absolute calibration required the application of the raster continuous scan technique and rejuvenated work on advanced antenna-calibration methods.

Employing its FSR, DSS 13 supported the detection of Beacon Monitor tones from both the MGS and DS1 spacecraft. This work migrated from DSS 26 to DSS 13 for programmatic reasons. The need to support the Beacon Monitor Operations concept (BMOX) helped shape the DSS 13 vision for increasingly autonomous operations.

DSS 13 was also regularly used for the development of the lunar neutrino detection technique. A JPL-UCLA collaboration, this exploratory program seeks to detect short electromagnetic pulses originating from particle interactions in the surface of the moon, thereby establishing a new approach to neutrino astronomy [Gorham et al., 2000].

### Current Advanced Technology Activities

DSS 13 currently participates in a number of advanced technology activities supported by the IPN-ISD Technology program.

The DSS 13 W-band Assessment is exploring the viability of the DSN BWG subnet at frequencies from 80-90 GHz. The motivations for this effort are:

- Technology development and demonstration for future space VLBI missions such as ARISE, as well as millimeter-wave VLBI in general
- Ground-based radio astronomical observations, world-class science aligned with NASA's Origins and Structure and Evolution of the Universe themes
- Gravity compensation measurements at Ka- and W-band in support of Ka-band implementation on the 70-m antennas
- Future DSN telecommunications at a high-data capacity, atmospheric transmission window between Ka-band and optical.

DSS 13 provides an ideal facility for gravity compensation work required by the DSN to utilize its 70-m antennas at Ka-band. The deformable flat plate has been installed at the station and will be used in conjunction with the Array Feed Compensation System (AFCS) for an extensive Ka-band test with Cassini. Moreover, since the scale of the gravity compensation problem goes like the diameter of an antenna measured in wavelengths, W-band provides a context for the investigation of the gravity compensation problem at a similar scale.

DSS 13 Autonomous Operations strives to develop a generic remote observing capability, to increase station utilization without increasing operational cost, to provide a rapid prototype, alternative approach that complements the DSN's automation effort, and to meet the automation needs of the station's science customers. This work is proceeding along a trajectory of increasing autonomy, from robust/remote operations through remote/unattended operations to autonomous/unattended operations. Robust/remote has been achieved. Remote/unattended-

unattended at the station but supervised by a remote, human intelligence has been demonstrated by trusted users that include the development team and GAVRT operators. The transition to remote/unattended as a general capability is occurring right now. It will be made available broadly to all interested users once they have been trained and certified by DSS 13 personnel.

Our goal is to achieve remote/unattended-unattended at the station, and supervised solely by machine intelligence by the end of fiscal year 2002. The culmination of DSS 13 autonomous operations, if achieved, would be the realization of the self-awakening station concept. Initially in a quiescent state, a self-awakening station would:

- 1) Detect unutilized capacity
- 2) Map a user to the opportunity
- 3) Plan an activity
- 4) Configure its hardware
- 5) Conduct the observation
- 6) Inform and deliver data to the selected user
- 7) Return to its quiescent state.

### Utilization

DSS 13 has traditionally been sponsored by the Technology, Engineering, and Plans and Commitments (DSN Science) offices of the InterPlanetary Network and Information Systems Directorate (formerly TMOD). A study was conducted this year to assess overall station utilization and to estimate station usage by each of its major sponsoring organizations. The study showed the station to be heavily utilized. In calendar year 2000, although only nominally operated five prime day shifts per week, DSS 13 supported 256 passes totaling 1894 observing hours. This averages to  $\approx 236$ , 8-hour (1894/8) passes or 4.5, 8-hour (236/52) passes per week. (This does not take into account downtime for maintenance, infrastructure development or major station reconfiguration.) The station is typically scheduled for one 8-hour mainte-

nance pass per week, although maintenance is often done on a non-interference basis in order to support more observation.

The assignment of users and projects to DSN Science, IPN-ISD Technology, and IPN-ISD Engineering was sometimes arbitrary. Observations conducted specifically in support of tasks funded by IPN-ISD Technology or called out in DSN Science Project Service Level Agreements (PSLAs) are unambiguous. However, new technology demonstrations that establish proof-of-principle prior to operational implementation, but regarded as advanced engineering rather than advanced technology, are labeled as IPN-ISD Engineering. For example, the Cassini Radio Science in-orbit checkout and beam aberration and point-ahead observations were assigned to this category.

The utilization study revealed a more balanced usage than anticipated:

• <i>DSN Science</i>	125 passes/1010 hours	49 % / 53 %
• <i>Technology</i>	68 passes/428 hours	26 % / 23 %
• <i>Engineering</i>	63 passes/456 hours	25 % / 24 %

### Future Directions and Challenges

DSS 13 will continue to be guided by the vision that has defined its evolution for the last three years. This is based on frequency agility, the development of high-frequency capability, and an increasingly autonomous station concept. We hope to significantly expand the scope of the W-band activity. Preliminary results from the W-band assessment indicate that a serious effort must be made to achieve the aperture efficiency required to be an effective instrument at millimeter wavelengths. Options include improving the surface figures of the main reflector, subreflector, and intermediate mirrors and applying compensation techniques such as the DFP or, perhaps, a deformable subreflector. We hope to apply the new closed-loop pointing technologies that are currently being developed for precise Ka-band blind pointing. We also hope to

be active in advanced antenna calibration; DSS 13 is the natural site for the development of the methodologies and instrumentation needed for high-data rate, continuous-scan calibration techniques.

The station also must face a number of challenges. Can it continue to serve its canonical role without renewing its downlink telemetry capability? DSS 13 should possess prototypes of the DSN's emerging telemetry engines: the Downlink Telemetry and Tracking subsystem (DTT) and the Radio Science Receiver (RSR), an upgraded version of the FSR capable of two-channel tone extraction and telemetry arraying. Should the station diversify its user base by supporting occasional operational users, risking its relaxed flavor of configuration control and freedom from the rigorous demands of flight project customers? If DSS 13 can meet these challenges, the station will continue to be a rich, important, and unique asset of the DSN well into the next decade.

## References

- [1] Smith, J. G., "Proposed Upgrade of the Deep Space Network Research and Development Station," *TMO Progress Report 42-88*, 1986.
- [2] Britcliffe, M. et al., "DSS-13 Beam Waveguide Antenna Project Phase 1 Final Report," *JPL D-8451*, 1991.
- [3] Clauss, R. C., and Smith, J. G., "Beam Waveguides in the Deep Space Network," *TMO Progress Report 42-88*, 1986.
- [4] Levin, S., and Hoffine, D., "Measuring Magnetic Fields in Stellar Nurseries," *TMOD Technology and Science Program News, Issue 11*, 2000\*
- [5] Levin, S. et al., "Measuring the Magnetic Field Strength in L1498 with Zeeman-Splitting Observations of CCS," *ApJ*, 555, 2001.
- [6] Gorham, P. et al., "Toward Radio Detection of Ultrahigh-Energy Neutrinos Using NASA's Deep Space Network," *TMOD Technology and Science Program News, Issue 12*, 2000\*

\* The InterPlanetary Network program overview and related features are located at: <http://tmot.jpl.nasa.gov>. For all issues of this newsletter, click Program Overview Information and, on the resulting page, click IPN-ISD News.



# Pre-college Student Contribution

## Cassini-Jupiter Microwave Observing Campaign (Cassini-JMOC)

### Introduction

The flyby of the Cassini spacecraft past Jupiter in December 2000 provided a unique opportunity to study Jupiter's radiation belts with high spatial resolution using a passive microwave radiometer that was built into the Cassini Radar Instrument. In a coordinated series of space-based and ground-based observations, named the Cassini-Jupiter Microwave Observing Campaign (Cassini-JMOC), Jupiter was observed at radio wavelengths during the Cassini encounter from November 2000 through March 2001 [Klein et al., 2000]. Cassini-JMOC had two science objectives:

- 1) Use ground-based observations to achieve in-flight calibrations of the Cassini radar receiver and thereby enhance the Cassini science at Saturn and Titan
- 2) Use the Cassini radar receiver to map Jupiter's synchrotron emission at a frequency above 10 gigahertz (GHz) and thereby derive the spatial distribution of very high energy electrons (greater than 20 megaelectronvolts) for the first time. Cassini-JMOC included an educational component that invited middle school and high school students to participate in the ground-based observations and data analysis.

Ground-based measurements of Jupiter's flux density relative to Venus and to a selection of radio sources were made to derive an accurate flux density for Jupiter at the spacecraft frequency (13.78 GHz). Precision measurements were also made at 2.3 GHz to monitor the time variability of the synchrotron radio emission from the Jovian radiation belts. These data are being merged with the ongoing NASA/JPL Jupiter Patrol [Klein et al., 1989] to study the intensity of the synchrotron emis-

sion at the time of the spacecraft observations and throughout the Cassini-JMOC observing period.

The educational objective was to engage pre-college students in scientific research. This was accomplished through the Goldstone-Apple Valley Radio Telescope (GAVRT) science education partnership involving NASA, JPL and the Lewis Center for Educational Research located in Apple Valley, CA [Klein and Stewart, 1999]. The GAVRT team logged more than 500 hours observing Jupiter and calibration radio sources during the campaign. Twenty-six schools located in 13 states joined the Cassini-JMOC team and 2300 students participated. The GAVRT experience provides insight into the world of professional science and access to the scientific community because the students become valued participants of the science team.

### Maps of Synchrotron Emission at 2.2 Centimeters

The Cassini flyby of Jupiter provided a unique opportunity to accurately measure the Jovian synchrotron radiation at a short centimeter wavelength for the first time. Measurements at 2.2 centimeters (13.78 GHz) were successfully carried out the first week in January near the time of closest approach to Jupiter using the radiometer subsystem of the Cassini Radar Instrument. Twenty hours of data yielded 20 maps covering a complete rotation of Jupiter in horizontal polarization and another complete rotation in vertical polarization.

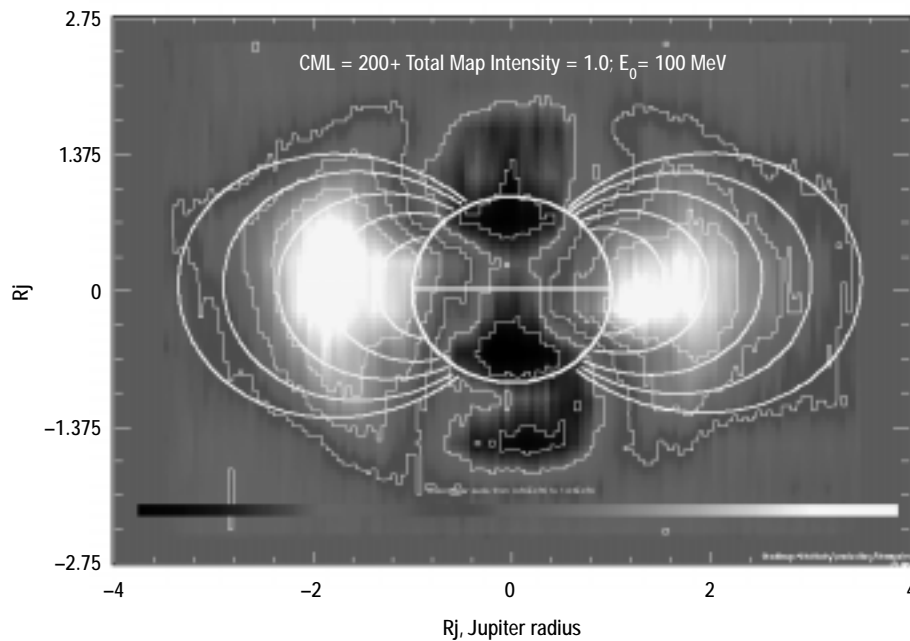
Synchrotron emission was clearly detected distinct from the thermal emission as evidenced by its polarization and spatial distri-

**Michael Klein,  
Scott Bolton,  
Michael  
Janssen, Steve  
Levin**

**Jim Roller and  
Bob McLeod  
Lewis Center  
for Educational  
Research,  
Apple Valley,  
California**

*The GAVRT experience provides insight into the world of professional science and access to the scientific community.*

**Figure 1.**  
Cassini spacecraft  
maps synchrotron  
emission from  
Jupiter's radiation  
belts



bution. Figure 1 is a preliminary map of this radio frequency emission from Jupiter's radiation belts as reported by Janssen et al. [2001]. These space-based data produced the first high-resolution maps of Jupiter's synchrotron emission at short centimeter wavelengths. The maps are important because they will provide unique information on the highest energy electrons in the magnetosphere. Earth-based radio telescopes have not produced accurate measurements of the synchrotron radiation at wavelengths this short because of the difficulty in separating atmospheric thermal emission from the synchrotron radiation, which is extremely weak compared to Jupiter's thermal emission at wavelengths shorter than  $\approx 6$  cm.

The total intensity derived by spatially integrating and then combining the two orthogonally polarized maps at 2.2 cm is only about one-sixth the intensity that was predicted from a computational model of the synchrotron radiation (Levin et al., 2001). The implications of these space-based results are discussed by Bolton and Gulkis (2001) and Janssen et al. (2001).

#### **DSN and GAVRT Observations at 13, 3.5 and 2.2 cm**

In addition to the space observations, Cassini-JMOC included ground-based observations of Jupiter's synchrotron radiation at several wavelengths using the VLA (operating at 20 and 90 cm). Also included was a combination of the GAVRT antenna and NASA's Deep Space Network operating at frequencies in the 13-, 3.5-, and 2.2-cm bands. We anticipate that by combining the space-based results with the ground-based measurements, our understanding of the energy spectrum and distribution of relativistic electrons trapped in Jupiter's radiation belts will be considerably improved.

Jupiter's synchrotron emission is known to be time-variable and there is plausible evidence that the observed variations are correlated with changes in solar wind parameters, for example, solar wind plasma density (Bolton et al., 1989). The Cassini encounter with Jupiter occurred as solar activity approaches the peak in the current eleven-year cycle. The last large-scale (greater than 20 percent) increase in Jupiter's synchrotron flux density was observed in the winter of 1989-90, just about eleven years ago. The GAVRT obser-

variations at 13 cm (2.295 GHz) were primarily made to monitor the time variations of the synchrotron emission from the radiation belts throughout the Cassini-JMOC observing period, but especially near the time of the spacecraft observations in the first week of January. The GAVRT data were merged with the ongoing NASA/JPL Jupiter Patrol to improve the sensitivity and time resolution of the resulting data. The results are shown in Figure 2.

The upper panel in Figure 2 shows the 30-year history of changes in the microwave radio emission from the radiation belts in the 11-13 cm bands. Changes up to 30 percent in the intensity of the microwave emission are clearly evident including the sudden outburst attributed to the impact of the Comet Shoemaker-Levy 9 in July of 1994. The lower panel is an enlarged view of the last two years of the data that includes the Cassini-JMOC observations. The open circles are NASA/JPL Jupiter Patrol observations made

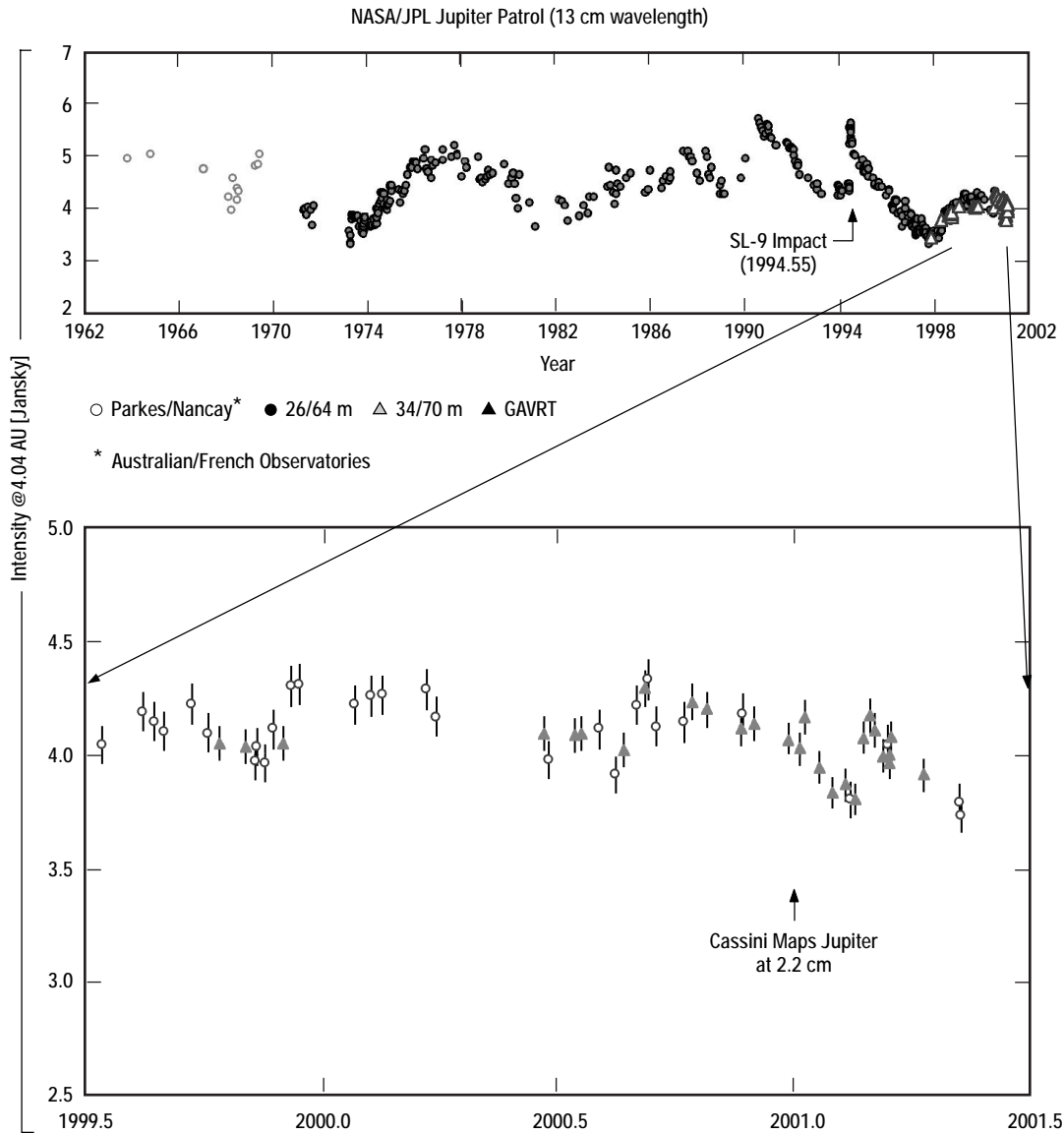


Figure 2. Variations in the intensity of microwave radio emission from Jupiter's radiation belts

*GAVRT Schools &  
Teachers on the  
Cassini-JMOC  
Team*

Ballard Junior High  
School  
Huxley, IA  
*S. Barth,  
D. Williams*

Barton Junior  
High School  
Buda, TX  
*D. Keel*

Brewton  
Middle School  
Brewton, AL  
*C. Brown,  
D. Goldwin*

Brownstown Central  
Brownstown, IN  
*R. Slaton*

Camden  
Middle School  
Camden, SC  
*K. Dozier*

Carver  
High School  
Columbus, GA  
*L. Richardson*

Cherokee County High  
School  
Centre, AL  
*M. Miller*

Connect Middle School  
Pueblo, CO  
*L. Hawkins*

Don Benito  
Elementary  
Pasadena, CA  
*L. Bush*

East High School  
Erie, PA  
*R. Fetzner*

George County Middle  
School  
Lucedale, MS  
*J. Mills, D. Wilson*

with DSN antennas. GAVRT team observations are represented by filled triangles. The relative 1-sigma uncertainty of the measurements is  $\approx 2\%$ . Note the excellent agreement between the two sets of data.

The intensity of Jupiter's synchrotron emission leading up to the Cassini encounter tends to be relatively flat throughout 1999 and 2000 superimposed with modest intensity increases ( $\approx 7\%$ ) in December 1999 and August 2000. The intensity was "near normal" from October through the first week in January when Cassini mapped the radiation belts at 2.2 cm. The 13-cm radio emission then appears to go through an 8% "dip" lasting from mid-January through mid-February. There is currently no explanation for this rather unique event.

These events of moderate short-term intensity variations appear to be intrinsic to Jupiter and not caused by systematic errors in calibration or by discrete background radio sources the planet passes during its 12-year orbital path along the ecliptic. Evidence of short-term variations in Jupiter's synchrotron radio emission have been reported in the past. There is hope that the intensity fluctuation in January 2001 will reveal new insights about Jupiter's inner radiation belts. This is expected to occur when the Cassini-JMOC results are compared with the in situ particle and field measurements collected by the Cassini and Galileo spacecraft during the Cassini flyby.

#### **GAVRT Observations of Jupiter at 13.8 GHz (2.2 cm)**

The Cassini-JMOC ground-based observations of Jupiter at 13.8 GHz were made simultaneously with the spacecraft observations to permit accurate ground-based radio astronomy flux calibration to be transferred to the Cassini radar receiver using Jupiter as a common reference source. The goal of

Cassini-JMOC is to calibrate the Jupiter flux density at 13.8 GHz with a 1-sigma absolute accuracy of 4 percent or better.

The GAVRT team measured the ratio of Jupiter relative to six calibration sources that were selected to mitigate different sources of random and systematic errors. The observed ratios were used to calculate the effective disk temperature of Jupiter for each calibrator. The results are shown in Figure 3. The error bars are one-sigma errors calculated from the scatter of multiple ratio measurements for each calibration source. The average of the six values of the effective disk temperature shown in the figure is 165.3 plus or minus 7.3 kelvin (K).

It is important to note these results are preliminary because additional calibration work is continuing through the remainder of 2001. The average disk temperature and error estimate will be modified as additional information is gathered to reduce the systematic error budget. Most notable of these will be the results of a new set of observations designed to map the brightness distribution of 3C405 and 3C274 at 13.8 GHz using a "raster scan" technique developed by Richter and Rochblatt (1997). The microwave spectra of the calibration sources will also be updated with new results from the National Radio Astronomy Observatory (NRAO) and improved model calculations of the microwave spectrum of Venus will be applied. The anticipated result of these and other updates will be to reduce the 7.3 K relative error and achieve an absolute error in the range of 2-4%.

Evaluating and reducing systematic errors of the radiometer subsystem will improve the capability of the Cassini Radar instrument to map the 2.2-cm emission from the surface of Titan and the rings and atmosphere of Saturn. The radar experiment is designed to penetrate the clouds of Titan and image the surface. The passive radiometer data will provide additional information to identify the location, extent, and compo-

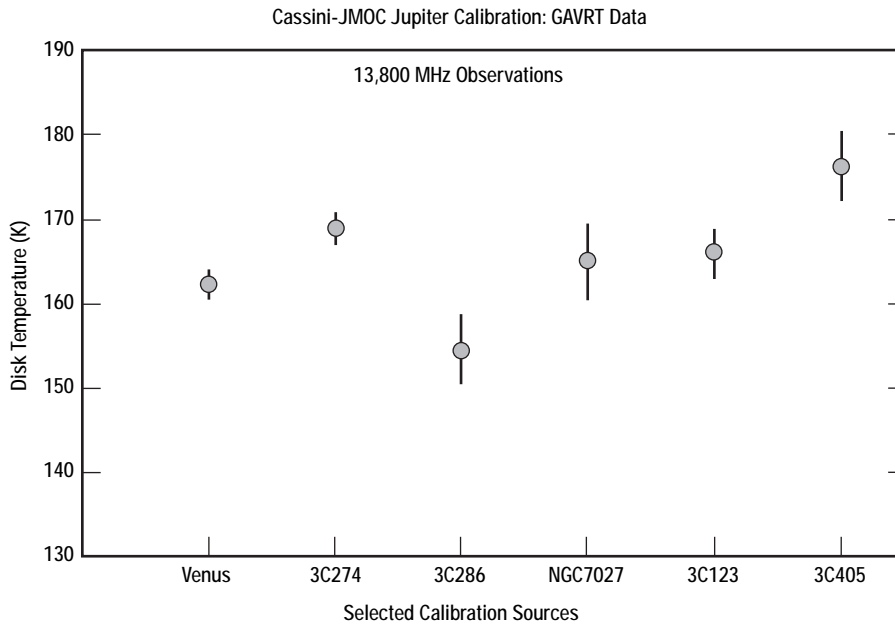


**Figure 3.**  
GAVRT  
measurements of  
the effective disk  
temperature of  
Jupiter at 13,780  
MHz

*GAVRT Schools &  
Teachers continued*

Glendora High School  
Glendora, CA  
*R. El Yousef*

Harborside School  
San Diego, CA  
*B. Arie*

Lakes Middle School  
Couer d'Alene, ID  
*C. Lind*

Academy for  
Academic Excellence  
Apple Valley, CA  
*K. Gay, M. Huffine,  
C. Hinojosa,  
D. MacLaren,  
D. Dorcey*

Mesquite  
Elementary School  
Apple Valley, CA  
*L. Smith*

Mojave Mesa  
Elementary School  
Apple Valley, CA  
*M. Deppe, M. Face*

Oak Mountain Middle  
School  
Birmingham, AL  
*A. Walker*

Opelika Middle School  
Opelika, AL  
*F. Seymore,  
M. Matin*

sition of surface features that the radar is likely to detect. To be effective, the absolute calibration accuracy must be in the 2–4% range. The team is confident that this objective will be met with the combination of the Cassini-JMOC data and the additional calibration sequences that are being planned.

**GAVRT Members of the Cassini-JMOC Team**

The Cassini-JMOC could not have accomplished the ground-based observing objectives without the dedicated work of the GAVRT teachers and their students. The interest and enthusiasm of the GAVRT team was a driving force to complete multiple observing sessions each week throughout the campaign. As it turned out, the repetitive observations were needed to detect the short-term dip in the 13-cm total intensity data. These important members of the Cassini-JMOC team and their schools were recognized at a special event held at JPL on May 4. Students and teachers from four GAVRT schools presented the GAVRT Team Report [C-JMOC 2001] to JPL Director, Dr. Charles Elachi, also a Principal Investigator for the Cassini Radar Instru-

ment. Moreover, the team has been awarded a NASA Group Achievement Award for 2001 and each of the 41 participating GAVRT teachers is on the list of recipients.

**Acknowledgments**

The authors gratefully acknowledge the Radio Astronomy and Radar Group and the technical staff at the Venus Development Site for their dedicated support of the GAVRT project and the Jupiter Patrol observations at Goldstone.

**References**

- [1] Bolton, S. J., S. Gulkis, M.J. Klein, I. de Pater, and T.J. Thompson, "Correlation Studies Between Solar Wind Parameters and the Decimetric Radio Emission From Jupiter," *J. Geophys. Res.*, 94, No. A1, 121, 1989.
- [2] Bolton, S. J. and S. Gulkis, "Jupiter's Synchrotron Emission: Unveiling the Jovian inner radiation belts through modeling and observation," *Fifth International Workshop of Planetary and Solar Radio Emission, Graz, Austria, April 1-4, 2001.*
- [3] *Cassini-Jupiter Microwave Observing Campaign: GAVRT Team Report: Prepared at the Lewis Center for Educational Research, Apple Valley, CA, and the Jet Propulsion Laboratory, Pasadena, CA, May 4, 2001.*

*GAVRT Schools & Teachers continued*

Ramona Middle School  
LaVerne, CA  
*M. Rodgers,  
D. Swinney  
M. Rasmussen,  
S. Massoudi*

Redlands East  
Valley High School  
Redlands, CA  
*J. Monaco*

Sanford Middle School  
Opelika, AL  
*F. Ware*

St. Mary's School  
Medford, OR  
*H. Bensei,  
J. Sokolowski*

Strong Vincent High  
School  
Erie, PA  
*D. Beard,  
C. Tattersail*

University Public  
School  
Detroit, MI  
*R. Rohn*

Vista Campana Middle  
School  
Apple Valley, CA  
*L. Hoegerman*

- [4] Janssen, M.A., S. J. Bolton, S. M. Levin, R. Sault, M. J. Klein, S. Gulkis, M. D. Hofstadter, C. Elachi, W. T. K. Johnson, A. Bunker, E. J. Gudim, G. A. Hamilton, O. Liepack, L. E. Roth, R. D. West, T. Bastian, G. Dulk, Y. Leblanc, R. Thorne, J. P. Roller and R. K. McLeod. "Cassini Radar/Radiometer and VLA Observations of Jupiter's Synchrotron Emission," *Fifth International Workshop of Planetary and Solar Radio Emission, Graz, Austria, April 1-4, 2001.*
- [5] Klein, M.J., T.J. Thompson and S.J. Bolton, "Systematic observations and correlation studies of variations in the synchrotron radio emission from Jupiter," in *Time-Variable Phenomena in the Jovian System*, edited by M.J.S. Belton, NASA SP 494, 151, 1989.
- [6] Klein, M. J. and J. M. Stewart, "The Goldstone-Apple Valley Radio Telescope: A Partnership in Science Education," *TMOD Technology*

and Science Program News, No. 10, 5-6, July 1999.\*

- [7] Klein, M. J., S. J. Bolton and M. A. Janssen, "GAVRT students contribute to the Cassini Millennium Flyby of Jupiter," *TMOD Technology and Science Program News, No. 12, 29-32, June 2000.\**
- [8] Levin, S. M., S. J. Bolton, S. Gulkis, M. J. Klein, B. Bhattacharya and R. M. Thorne, "Modeling Jupiter's synchrotron radiation," *Geophys. Res. Letters, 28, No. 5, 903-906, March 1, 2001.*
- [9] Richter, P.H. and D. J. Rochblatt, "A Microwave Performance Calibration System for NASA's Deep Space Network Antennas: Part 1: Assessment of Antenna Gain and Pointing and Calibration of Radio Sources," *Proceedings 10th International Conference on Antennas and Propagation, Vol. 1, pp 1.142-1.149, April 14-17, 1997.*



*This newsletter is a publication of JPL's InterPlanetary Network and Information Systems Directorate (IPN-ISD). The IPN Program is managed by Jim Lesh and the Science Program by Michael J. Klein.*

*\* The InterPlanetary Network program overview and related features are located at: <http://tmot.jpl.nasa.gov>. For all issues of this newsletter, click Program Overview Information and, on the resulting page, click IPN-ISD News.*

*To add or delete your name from the IPN News contact Cruzita Abellana at 818-354-9071 or email [Cruzita.Abellana@jpl.nasa.gov](mailto:Cruzita.Abellana@jpl.nasa.gov)*

*Managing Editor Charles T. Stelzried  
Associate Editor Christopher A. Weaver,  
Documentation Services  
Design and Layout Design Services*



National Aeronautics and  
Space Administration  
Jet Propulsion Laboratory  
California Institute of Technology  
Pasadena, California

JPL 410-62, Issue No. 14, 9/01

IPN-ISD Technology Program Office, MS 303-407  
Jet Propulsion Laboratory  
4800 Oak Grove Drive  
Pasadena, California 92209-8099